Characterization of Pauli Errors in Entangled Link Channel via Purification Protocol on IBM Quantum Device

Keio University Faculty of Environment and Information Studies

Bachelor's Thesis(Academic Year 2023)

Hikaru Yokomori

Abstract

The characterization of an entangled link in a quantum network is crucial for the distribution of entangled states in future quantum networks. However, a key challenge lies in the resource cost and potential application stoppage due to the link consumption via state tomography performance. This study focuses on implementing and verifying a new approach proposed by Maity et al [33], aiming to characterize the link using a purification protocol.

In this project, we conducted a characterization of a simulated entangled link, assuming a Werner state, on an actual quantum device. The focus was on implementing mentioned Maity et al's work, which employs different Pauli purification schemes. The obtained results were compared, providing insights into the effectiveness of the purification process.

The outcomes of the study contribute to the ongoing discussions about the challenges and possibilities in quantum network development. The results also shed light on the potential performance of quantum systems under different scenarios. Moreover, the use of the purification protocol presents itself as a valuable tool for testing the capabilities of quantum systems.

Looking forward, this study opens avenues for future research, considering various scenarios for simulating entangled links. It also prompts exploration of the protocol's adaptability to different quantum system setups. By addressing these aspects, we can enhance our understanding of entangled links and optimize the utilization of purification protocols in quantum networks.

Keywords :
1. Quantum Network, 2. Quantum Purification, 3. Entangled Link, 4. Error Characterization

Contents

List of Figures

Chapter 1

Introduction

Ever since the term, “Quantum Computer” was proposed by Richard Feynman in 1981 [15], the race to achieve useful fault tolerant quantum computer and its application have been tremendously competitive and exciting. One of the biggest innovative and revolutionary adaptation would be the quantum network where we construct a network that transmits quantum information, opening up vast new world of real world application from security, sensing, to scaling of quantum computer itself.

In the future quantum network, entangled quantum system is presumed to be used as links between nodes. For application to run seamlessly, characterizing the errors within the link is important. In the paper by Maity et al from Okinawa Institute of Science and Technology (OIST), they proposed a relatively new approach of characterizing the error, Pauli Errors in particular [33]. This approach uses the purification protocol [3], where two parties each share one system of the two entangled state and exchange classical measurement result of one entangled state after doing a certain operation. The original intention of the protocol was to improve the entangled link and detect Pauli errors. They derived an equation that uses the usually throne away, measurement results to estimate the error parameters. Such approach, not only reduces the cost of error characterization, but allows us to prevent stopping the application its self. This killing two birds with one stone approach could have potential in advancing the evaluation and application of the entangled link in quantum network.

This paper aims to explain how I tackled two problems in different layers; one being how I can characterize the errors efficiently without stopping the application, using the protocol by Maity et al and second being the actual implementation of the idea on real device to see if it actually works.

1.1 Thesis Structure

This thesis explains my project as follows. First, I covered the context of the project, the background in which what I was talking about. It explains the concept of quantum network with the basic quantum information knowledge needed to understand my problem (Ch. 2). Then, I clarified two main challenges that I tackled in this project, introducing the traditional and the new approach (Ch. 3). In the following chapter, I introduced the setups to conduct the proposed approaches and how I evaluated them (Ch. 4). After that, I shared and discussed each results of the setups (Ch. 5). Then finally, I will introduce the conclusion from the discussion and possible works to be done in the future (Ch. 6).

Chapter 2

Background

This chapter aims to explain the context of my project which are entangled link in quantum network followed by classical network and the basic knowledge needed to understand the problem which I will be introducing in the following chapter.

2.1 Classical Network and Communication

Classical network today allows us to communicate around the world by transmitting information. Communication occurs when a sender encodes information into a format suitable for transmission, sends it through a channel, and then a receiver decodes it. This channel in network is referred to as the link. Take the electrical telegraph; a message is encoded by a Morse key operator, transmitted via electrical wires, and decoded at the destination.

There are two main types of signal transmission: analog and digital. Analog signals are continuous waves representing information such as sound and temperature, familiar to human senses but prone to noise and distortion when processed by machines, making them challenging to duplicate accurately.

On the other hand, digital signals use discrete values for encoding, offering more resilience to noise and easier replication. The precision of digital signals depends on the sampling rate. With fewer states required to represent data, the digital system becomes more efficient. For instance, a signal off for one second can signify '0', while on for three seconds can mean '1'. This unit, known as a bit, is the fundamental element of digital communication, representing binary choices like true/false or on/off. The simplicity and efficiency of digital signals comes in handy when combined with the binary notation system, an elegant language of zeros and ones.

Binary notation uses just two characters, 0 and 1, allows us to represent various values with bits. For instance, 1 bit can indicate 2 values (0 or 1), 2 bits can express 4 values (00, 01, 10, or 11), and 3 bits can yield 8 values (000 to 111). In general, N bits can represent 2^N values.

Our everyday counting system, the decimal system, uses ten digits (0 through 9) and is termed decimal notation. While binary notation forms the backbone of digital communication, understanding its relationship with the more familiar decimal system can further illustrate its use and efficiency. Decimal numbers can be converted into binary. For example, the decimal 1024 breaks down into $1 \times 10^3 + 0 \times 10^2 + 2 \times 10^1 + 4 \times 10^0$. This is a base-10 system. In binary, base 2, the number 1001 is $1 \times 2^3 + 0 \times 2^2 + 0 \times 2^1 + 1 \times 2^0$, which equals 9 in decimal notation. We prefer bits for their resistance to noise and simplicity in encoding, decoding, and processing. Using the bits, we transmit information and communicate on classical network.

Physical laws shape the way we process and communicate information. Classical communication is based on classical physics and processes information in traditional ways. In contrast, quantum communication uses quantum mechanics, quationing with the most fundamental understanding of nature we have today. This approach is increasingly relevant as technological advancements near the limits set by classical physics, a trend that Moore's Law, with its prediction of the exponential increase in microchip transistors, helps illustrate. One key difference in quantum mechanics is the principle of superposition, which allows quantum bits (qubits) to exist in multiple states simultaneously, unlike classical bits that are strictly binary, being either '0' or '1', 'on' or 'off'. This principle expands the realm of quantum computation, enabling the transmission of quantum information across quantum networks. Quantum network creates vast new world of different various applications that were not possible in classical network.

2.2 Quantum Computation

This chapter will explain the basics of quantum computation which most of the topics are selected from the text book 'Quantum Communications' [21], made by our lab, Advancing Quantum Architecture research group at Keio University's Shonan Fujisawa Campus (AQUA) and 'Dancing with Qubits' [45].

2.2.1 Qubit

In quantum computing, as mentioned, the primary unit is the ***qubit***, whereas classical computing is based on classical bits. Classical bits are always in a deterministic state of either 0 or 1. While qubits, on the other hand, can exist probabilistically in states between 0 and 1, such as being 50% in state 0 and 50% in state 1. This unique condition is known as the superposition. I do not prefer to use analogy, rather use examples, but to give intuitive image, I will sometimes do so. To illustrate the concept of superposition, consider the analogy of a spinning coin. When a coin is flipped and is in the air, it is neither in a state of 'heads' nor 'tails', but rather in a mix of both. This state continues until the coin lands, at which point it assumes a definite state. This is similar to a qubit in superposition, which exists in a combination of both 0 and 1 states, embodying the potential for either state. Only upon measurement does the qubit 'collapse' into a definitive state, similar to the coin settling on either heads or tails. This qubit can be represented in various notations depending on their appropriate use.

Bra-ket and Vector Notation

Single qubit's quantum state, is often represented using bra-ket notation, sometimes also called the Dirac notation, introduced by Paul Dirac [11]. It is expressed as

$$|\psi\rangle = \alpha\,|0\rangle + \beta\,|1\rangle\,. \tag{2.1}$$

$|\psi\rangle$ ("ket-psi") is used commonly to represent a quantum state. Here, $|0\rangle$ ("ket-zero") and $|1\rangle$ ("ket-one"), are the foundational computational basis or Pauli Z basis states. Basis is a set of orthogonal quantum states that can be combined to represent any state in a quantum system. In vector notation, these computational basis states can be represented as

$$|0\rangle = \begin{bmatrix}1\\0\end{bmatrix}, \quad |1\rangle = \begin{bmatrix}0\\1\end{bmatrix}. \tag{2.2}$$

The coefficients α and β in equation 2.1, are complex probability amplitudes, dictating the qubit's likelihood of being in either $|0\rangle$ or $|1\rangle$. To intuitively grasp probability amplitudes, one can consider the analogy of ocean waves. The height of a wave represents its amplitude, which in the quantum realm equates to the probability amplitude of a qubit. A taller wave signifies a higher probability amplitude, indicating a greater chance of finding the qubit in a particular state when measured. Just as waves can interfere constructively or destructively, affecting their overall height, probability amplitudes can combine in quantum states, leading to varying probabilities for different outcomes. These probability amplitudes must satisfy the normalization condition for a single qubit system which is

$$|\alpha|^2 + |\beta|^2 = 1. \tag{2.3}$$

To confirm a state's normalization, the inner product of the state with itself should be 1.

Inner product is the dot product in linear algebra. The ket, $|\psi\rangle$, has a corresponding bra, $\langle\psi|$, which is the complex conjugate transpose (also known as Hermitian Conjugate or adjoint) of the matrix, represented as

$$\langle\psi| = (|\psi\rangle)^\dagger = \begin{bmatrix}\alpha\\\beta\end{bmatrix}^\dagger = \begin{bmatrix}\alpha^* & \beta^*\end{bmatrix}. \tag{2.4}$$

For two quantum states, $|\psi\rangle = \alpha\,|0\rangle + \beta\,|1\rangle$ and $|\phi\rangle = \gamma\,|0\rangle + \delta\,|1\rangle$, the inner product is

$$\langle\phi|\psi\rangle = \begin{bmatrix}\gamma^* & \delta^*\end{bmatrix}\begin{bmatrix}\alpha\\\beta\end{bmatrix} = \alpha\gamma^* + \beta\delta^*. \tag{2.5}$$

Inner product of a quantum state with itself could be represented as

$$\langle\psi|\psi\rangle = \begin{bmatrix}\alpha^* & \beta^*\end{bmatrix}\begin{bmatrix}\alpha\\\beta\end{bmatrix} = \alpha\alpha^* + \beta\beta^* = |\alpha|^2 + |\beta|^2. \tag{2.6}$$

Going back to the normalization of the quantum state, equation 2.6 must equal to 1, as equation 2.3 for a state has to satisfy the condition.

Using the equation 2.2, the vector representation of $|\psi\rangle$ in the computational basis could be written as

$$|\psi\rangle = \alpha \begin{bmatrix} 1 \\ 0 \end{bmatrix} + \beta \begin{bmatrix} 0 \\ 1 \end{bmatrix} = \begin{bmatrix} \alpha \\ \beta \end{bmatrix}. \tag{2.7}$$

In addition to the Pauli Z basis, a qubit's state can be represented in various other bases. Pauli X basis is one of them and is made of the states $|+\rangle$ ("ket-plus") and $|-\rangle$ ("ket-minus"). These states are defined as equal superposition of the computational basis states as

$$|+\rangle = \frac{1}{\sqrt{2}}(|0\rangle + |1\rangle), \quad |-\rangle = \frac{1}{\sqrt{2}}(|0\rangle - |1\rangle). \tag{2.8}$$

The states $|+\rangle$ and $|-\rangle$ in vector notation are given by

$$|+\rangle = \frac{1}{\sqrt{2}}(|0\rangle + |1\rangle) = \frac{1}{\sqrt{2}}\left(\begin{bmatrix} 1 \\ 0 \end{bmatrix} + \begin{bmatrix} 0 \\ 1 \end{bmatrix}\right) = \frac{1}{\sqrt{2}}\begin{bmatrix} 1 \\ 1 \end{bmatrix}, \tag{2.9}$$

$$|-\rangle = \frac{1}{\sqrt{2}}(|0\rangle - |1\rangle) = \frac{1}{\sqrt{2}}\left(\begin{bmatrix} 1 \\ 0 \end{bmatrix} - \begin{bmatrix} 0 \\ 1 \end{bmatrix}\right) = \frac{1}{\sqrt{2}}\begin{bmatrix} 1 \\ -1 \end{bmatrix}. \tag{2.10}$$

Thus, a single qubit state $|\psi\rangle$ in the Pauli X basis could be expressed as

$$|\psi\rangle = \frac{\alpha + \beta}{\sqrt{2}} |+\rangle + \frac{\alpha - \beta}{\sqrt{2}} |-\rangle. \tag{2.11}$$

The normalization condition for the probability amplitudes will be

$$\frac{|\alpha + \beta|^2}{2} + \frac{|\alpha - \beta|^2}{2} = 1 \tag{2.12}$$

Another example of basis is the Pauli Y basis, consisting of the states $|i\rangle$ and $|-i\rangle$. These are defined as

$$|i\rangle = \frac{1}{\sqrt{2}}(|0\rangle + i\,|1\rangle), \quad |-i\rangle = \frac{1}{\sqrt{2}}(|0\rangle - i\,|1\rangle). \tag{2.13}$$

In the vector notation, represented as

$$|i\rangle = \frac{1}{\sqrt{2}}(|0\rangle + i\,|1\rangle) = \frac{1}{\sqrt{2}}\left(\begin{bmatrix} 1 \\ 0 \end{bmatrix} + i\begin{bmatrix} 0 \\ 1 \end{bmatrix}\right) = \frac{1}{\sqrt{2}}\begin{bmatrix} 1 \\ i \end{bmatrix}, \tag{2.14}$$

$$|-i\rangle = \frac{1}{\sqrt{2}}(|0\rangle - i\,|1\rangle) = \frac{1}{\sqrt{2}}\left(\begin{bmatrix} 1 \\ 0 \end{bmatrix} - i\begin{bmatrix} 0 \\ 1 \end{bmatrix}\right) = \frac{1}{\sqrt{2}}\begin{bmatrix} 1 \\ -i \end{bmatrix}. \tag{2.15}$$

Thus, a single qubit state $|\psi\rangle$ in the Pauli Y basis could be expressed as

$$|\psi\rangle = \frac{\alpha - \beta i}{\sqrt{2}} |i\rangle + \frac{\alpha + \beta i}{\sqrt{2}} |-i\rangle, \tag{2.16}$$

where

$$\frac{|\alpha - \beta i|^2}{2} + \frac{|\alpha + \beta i|^2}{2} = 1 \tag{2.17}$$

is the normalization condition for the probability amplitudes. It is important to notice that these are all same single qubit state, but are description of them in different basis. This will be important later in the measurement and obtainment of the states knowledge.

Bloch Sphere Representation

A single qubit's quantum state can also be intuitively visualized using the Bloch Sphere [5]. The sphere maps the entire range of a qubit's potential states onto its surface, going beyond the binary limitations of classical bits. Figure 2.1 provides an illustration of the Bloch Sphere. The state of a qubit $|\psi\rangle$ can be any point on the sphere's surface, indicating the vast array of superposition. The angles θ measures the angle from the positive Z-axis, and ϕ from the positive X-axis on the XY-plane. Mathematically, this is expressed as

$$|\psi\rangle = \cos\frac{\theta}{2}|0\rangle + e^{i\phi}\sin\frac{\theta}{2}|1\rangle. \tag{2.18}$$

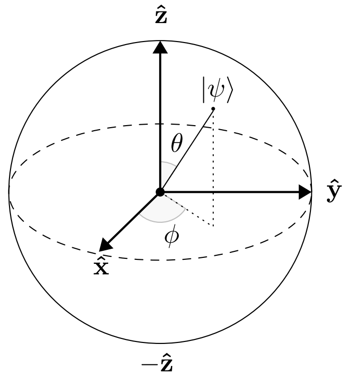

Figure 2.1: Example illustration of $|\psi\rangle$ on the Bloch Sphere

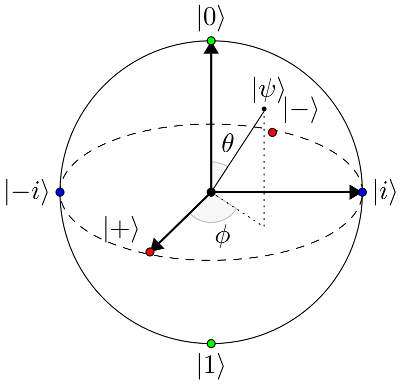

Figure 2.2: Bloch Sphere representation of each Pauli basis

This formula directly ties into our previous discussion on probability amplitudes from equation 2.1. The components $\cos\frac{\theta}{2}$ and $e^{i\phi}\sin\frac{\theta}{2}$ can be seen as geometric representations of the probability amplitudes α and β.

Each Pauli basis states can be plotted on Bloch Sphere as shown in Figure 2.2. On this sphere, the Pauli X basis states, $|0\rangle$ and $|1\rangle$, are positioned at the north and south poles. States in the Pauli X basis, $|+\rangle$ and $|-\rangle$, are located on the equator. Specifically, $|+\rangle$ corresponds to a point on the equator at $\theta = 90°$ and $\phi = 0°$. Similarly, $|-\rangle$ is also on the equator but at $\theta = 90°$ and $\phi = 180°$. In the case of the Y-basis, $|i\rangle$ and $|-i\rangle$, these states are represented as points on the equator as well but at different angles ϕ. $|i\rangle$ can be visualized at $\theta = 90°$ and $\phi = 90°$, while $|-i\rangle$ is at $\theta = 90°$ and $\phi = 270°$. Moreover, the Bloch Sphere is not just a static representation. It is a dynamic tool for visualizing quantum operations which will be introduced in later section.

Outer Product

Beyond bra-ket and vector notations, quantum states can be described using outer products. An outer product of a general state, denoted as $|\psi\rangle\langle\psi|$, provides a way to express the state as a matrix. This representation is particularly useful for describing the full knowledge of quantum systems. For a general state $|\psi\rangle$, its outer product can be written as

$$|\psi\rangle\langle\psi| = \begin{bmatrix}\alpha \\ \beta\end{bmatrix}\begin{bmatrix}\alpha^* & \beta^*\end{bmatrix} = \begin{bmatrix}|\alpha|^2 & \alpha\beta^* \\ \alpha^*\beta & |\beta|^2\end{bmatrix}. \tag{2.19}$$

Here, α and β are complex probability coefficients that describe the quantum state, from equation 2.1. This matrix representation captures the probabilities associated with measuring the state in the Pauli Z basis states $|0\rangle$ and $|1\rangle$. The outer products of the basis states $|0\rangle$ and $|1\rangle$ are

$$|0\rangle\langle 0| = \begin{bmatrix}1 \\ 0\end{bmatrix}\begin{bmatrix}1 & 0\end{bmatrix} = \begin{bmatrix}1 & 0 \\ 0 & 0\end{bmatrix}. \tag{2.20}$$

$$|1\rangle\langle 1| = \begin{bmatrix}0 \\ 1\end{bmatrix}\begin{bmatrix}0 & 1\end{bmatrix} = \begin{bmatrix}0 & 0 \\ 0 & 1\end{bmatrix}. \tag{2.21}$$

2.2.2 Multiple Qubits

When considering two classical bits, we can have 4 possible states; 00, 01, 10, 11. When considering 2 qubits, using the Bra-ket notation, we can have 4 possible states as well; $|00\rangle$, $|01\rangle$, $|10\rangle$, $|11\rangle$. Therefore, any general state of two-qubit could be written in bra-ket notation as

$$|\psi\rangle = \alpha\,|00\rangle + \beta\,|01\rangle + \gamma\,|10\rangle + \delta\,|11\rangle\,, \tag{2.22}$$

where α, β, γ, δ are the probability amplitudes. The normalization condition of the probability amplitudes is

$$|\alpha|^2 + |\beta|^2 + |\gamma|^2 + |\delta|^2 = 1. \tag{2.23}$$

Tensor Product

To write them in the vector notation, we have to use the tensor product in linear algebra. Suppose we have two states of two-qubit, $|A\rangle$ and $|B\rangle$, we can compute the tensor product of the two states as

$$|A\rangle \otimes |B\rangle = \begin{bmatrix} a_1 \\ a_2 \end{bmatrix} \otimes \begin{bmatrix} b_1 \\ b_2 \end{bmatrix} \equiv \begin{bmatrix} a_1 \begin{bmatrix} b_1 \\ b_2 \end{bmatrix} \\ a_2 \begin{bmatrix} b_1 \\ b_2 \end{bmatrix} \end{bmatrix} = \begin{bmatrix} a_1 b_1 \\ a_1 b_2 \\ a_2 b_1 \\ a_2 b_2 \end{bmatrix}. \tag{2.24}$$

The tensor product operation takes the first element of the first probability amplitude vector and multiply it with the whole second probability amplitude vector. Then takes the second element of the first probability amplitude vector and multiply it with the whole second probability amplitude vector. For example, In the vector notation each Pauli Z basis states for two-qubit can be written as follows using the tensor product from linear algebra;

$$|00\rangle = |0\rangle \otimes |0\rangle = \begin{bmatrix} 1 \\ 0 \end{bmatrix} \otimes \begin{bmatrix} 1 \\ 0 \end{bmatrix} = \begin{bmatrix} 1 \\ 0 \\ 0 \\ 0 \end{bmatrix}, \qquad |01\rangle = |0\rangle \otimes |1\rangle = \begin{bmatrix} 1 \\ 0 \end{bmatrix} \otimes \begin{bmatrix} 0 \\ 1 \end{bmatrix} = \begin{bmatrix} 0 \\ 1 \\ 0 \\ 0 \end{bmatrix}, \tag{2.25}$$

$$|10\rangle = |1\rangle \otimes |0\rangle = \begin{bmatrix} 0 \\ 1 \end{bmatrix} \otimes \begin{bmatrix} 1 \\ 0 \end{bmatrix} = \begin{bmatrix} 0 \\ 0 \\ 1 \\ 0 \end{bmatrix}, \qquad |11\rangle = |1\rangle \otimes |1\rangle = \begin{bmatrix} 0 \\ 1 \end{bmatrix} \otimes \begin{bmatrix} 0 \\ 1 \end{bmatrix} = \begin{bmatrix} 0 \\ 0 \\ 0 \\ 1 \end{bmatrix}. \tag{2.26}$$

We can use the tensor product for other more complicated states as well. For example we can use it for $|0\rangle$, $|1\rangle$, $|+\rangle$, $|-\rangle$ as

$$|0\rangle \otimes |+\rangle = \begin{bmatrix} 1 \\ 0 \end{bmatrix} \otimes \frac{1}{\sqrt{2}} \begin{bmatrix} 1 \\ 1 \end{bmatrix} = \frac{1}{\sqrt{2}} \begin{bmatrix} 1 \\ 1 \\ 0 \\ 0 \end{bmatrix}, \qquad |0\rangle \otimes |-\rangle = \begin{bmatrix} 1 \\ 0 \end{bmatrix} \otimes \frac{1}{\sqrt{2}} \begin{bmatrix} 1 \\ -1 \end{bmatrix} = \frac{1}{\sqrt{2}} \begin{bmatrix} 1 \\ -1 \\ 0 \\ 0 \end{bmatrix}, \tag{2.27}$$

$$|1\rangle \otimes |+\rangle = \begin{bmatrix} 0 \\ 1 \end{bmatrix} \otimes \frac{1}{\sqrt{2}} \begin{bmatrix} 1 \\ 1 \end{bmatrix} = \frac{1}{\sqrt{2}} \begin{bmatrix} 0 \\ 0 \\ 1 \\ 1 \end{bmatrix}, \qquad |1\rangle \otimes |-\rangle = \begin{bmatrix} 0 \\ 1 \end{bmatrix} \otimes \frac{1}{\sqrt{2}} \begin{bmatrix} 1 \\ -1 \end{bmatrix} = \frac{1}{\sqrt{2}} \begin{bmatrix} 0 \\ 0 \\ 1 \\ -1 \end{bmatrix}. \tag{2.28}$$

Product States

We refer to the tensor product of two local states as the global state. Global state that has the perfect knowledge of multiple local states are called the product state. For example, if we have two local states of qubit A and B, denoted as $|\psi\rangle_A = |0\rangle$ and $|\psi\rangle_B = |+\rangle$, the global state of both qubits, $|\psi\rangle_{AB}$, can be described as

$$|\psi\rangle_{AB} = |\psi\rangle_A \otimes |\psi\rangle_B = |0\rangle \otimes |+\rangle = \frac{1}{\sqrt{2}}(|00\rangle + |01\rangle). \tag{2.29}$$

We can obtain the knowledge of local states $|\psi\rangle_A$ and $|\psi\rangle_B$ from the global state $|\psi\rangle_{AB}$. When we are given a global state $|\psi\rangle_{AB} = \frac{1}{\sqrt{2}}(|00\rangle + |01\rangle)$, by writing the general state of qubit A and B as

$$|\psi\rangle_A = a_0\,|0\rangle + a_1\,|1\rangle\,, \qquad |\psi\rangle_B = b_0\,|0\rangle + b_1\,|1\rangle\,. \tag{2.30}$$

By forming the tensor product of these two states, we expand it as

$$|\psi\rangle_A \otimes |\psi\rangle_B = (a_0\,|0\rangle + a_1\,|1\rangle) \otimes (b_0\,|0\rangle + b_1\,|1\rangle) \tag{2.31}$$

$$= a_0b_0\,|00\rangle + a_0b_1\,|01\rangle + a_1b_0\,|10\rangle + a_1b_1\,|11\rangle\,. \tag{2.32}$$

To match the given global state $|\psi\rangle_{AB}$, the coefficients must satisfy the following conditions;

$$a_0b_0 = \frac{1}{\sqrt{2}}, \quad a_0b_1 = \frac{1}{\sqrt{2}}, \tag{2.33}$$

$$a_1b_0 = 0, \quad a_1b_1 = 0. \tag{2.34}$$

From these conditions, we can infer that $a_1 = 0$ since the global state does not contain $|10\rangle$ or $|11\rangle$. Therefore, the local state of qubit A simplifies to $|\psi\rangle_A = a_0\,|0\rangle$, to satisfy the normalization condition, $|a_0|^2 = 1$, which implies $a_0 = 1$. Thus, $|\psi\rangle_A = |0\rangle$. For qubit B, the local state $|\psi\rangle_B$ is determined by b_0 and b_1. Given that the amplitude of $|0\rangle$ and $|1\rangle$ in $|\psi\rangle_B$ are equal, we deduce that $b_0 = b_1 = \frac{1}{\sqrt{2}}$. Therefore, the local state of qubit B is

$$|\psi\rangle_B = \frac{1}{\sqrt{2}}\,|0\rangle + \frac{1}{\sqrt{2}}\,|1\rangle \tag{2.35}$$

$$= |+\rangle\,. \tag{2.36}$$

So, we could say that the given global state $|\psi\rangle_{AB}$ is a product state as we can obtain local states $|\psi\rangle_A$ and $|\psi\rangle_B$. This is not always the case, as introduced later in the chapter, there will be a global state that cannot obtain the full knowledge of the local states even though we have the full knowledge of the global states.

2.2.3 Quantum Circuit Representation

We use quantum circuit representation, which are intuitive and practical way, to work with quantum information (states) and operations. Single qubit quantum state, denoted as $|\psi\rangle$, in a quantum circuit, is represented by a horizontal wire. Various operation (gates) which will be introduced in the following section can be applied to the qubit state by inserting them along the wire. These gates alter the quantum state's properties or transform it into different basis states. The operations are performed from left to right for each qubit. Quantum circuits allow the construction of quantum algorithms and computations. The following is an example of a quantum teleportation protocol of a single qubit $|\psi\rangle$ which will be explained in later section. Figure 2.3 is a specific example of quantum protocol called quantum teleportation, using quantum operation.

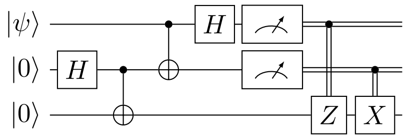

Figure 2.3: Quantum teleportation circuit

2.2.4 Execution of Quantum Operations (Unitary Gates)

In quantum computing, operations refer to the specific actions or transformations applied to quantum states, specifically we use what are known as unitary operations. These unitary operations, symbolized as $\boldsymbol{U}$, are not only fundamental but are distinguished by their reversibility, a characteristic essential for quantum algorithms. The reversal of a unitary operation is achieved through the application of its adjoint, represented as $\boldsymbol{U}^\dagger$. This reversibility is important because it enables the manipulation and control of qubit states without loss of information. Unitary operation in definition could be mathematically represented as

$$\boldsymbol{U}\boldsymbol{U}^\dagger = \boldsymbol{U}^\dagger\boldsymbol{U} = \boldsymbol{I}. \tag{2.37}$$

Here, $\boldsymbol{I}$ symbolizes the identity operator, an operator that leaves the state it acted upon unchanged. To construct the adjoint $\boldsymbol{U}^\dagger$ of a unitary matrix, we take the complex conjugate of each element in the matrix. Then we transpose the matrix, which involves flipping it across its diagonal as

$$U = \begin{bmatrix} U_{00} & U_{01} \\ U_{10} & U_{11} \end{bmatrix} \rightarrow \begin{bmatrix} U_{00}^* & U_{10}^* \\ U_{01}^* & U_{11}^* \end{bmatrix} = U^\dagger. \tag{2.38}$$

Given that quantum states are represented as vectors in a complex vector space, unitary operations correspond to matrices. These matrices, when applied to state vectors, alter their state without changing the overall probability (norm of the vector remains 1). Vector norm is a function that assigns a non-negative length or size to each vector in a vector space, which represents the vector's magnitude in that space, to preserve the probability amplitude condition.

As stated, the quantum gates in a quantum circuit represent quantum operations. In the circuit representation, a unitary operation is generally depicted as a box containing the symbol of the operation, acting on a horizontal line that represents a qubit. For example, a general unitary operation $\boldsymbol{U}$ on a single qubit can be represented as

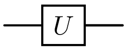

in a quantum circuit. In this circuit diagram, the horizontal line represents the quantum wire, indicating the qubit, and the box labeled $\boldsymbol{U}$ denotes the application of the unitary operation to the qubit. The flow of the circuit is from left to right, indicating the sequence of operations applied.

Identity Operation (I Gate)

As mentioned, the operation of doing nothing is called the identity operation. It is usually denoted $\boldsymbol{I}$. The matrix representation is

$$I = \begin{bmatrix} 1 & 0 \\ 0 & 1 \end{bmatrix}. \tag{2.39}$$

For example, when applied to the quantum states $|0\rangle$ and $|1\rangle$, leaves them unchanged and can be mathematically shown as

$$I|0\rangle = \begin{bmatrix} 1 & 0 \\ 0 & 1 \end{bmatrix} \begin{bmatrix} 1 \\ 0 \end{bmatrix} = \begin{bmatrix} 1 \\ 0 \end{bmatrix} = |0\rangle, \qquad I|1\rangle = \begin{bmatrix} 1 & 0 \\ 0 & 1 \end{bmatrix} \begin{bmatrix} 0 \\ 1 \end{bmatrix} = \begin{bmatrix} 0 \\ 1 \end{bmatrix} = |1\rangle. \tag{2.40}$$

Circuit representation

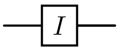

Pauli X Operation (X Gate): Bit Flip

Pauli X operation, also known as the quantum bit flip operation is denoted $\boldsymbol{X}$. This operation interchanges the state $|0\rangle$ to $|1\rangle$ and vice versa. The matrix representation is

$$X = \begin{bmatrix} 0 & 1 \\ 1 & 0 \end{bmatrix}. \tag{2.41}$$

Examples of the the operation

$$X|0\rangle = \begin{bmatrix} 0 & 1 \\ 1 & 0 \end{bmatrix} \begin{bmatrix} 1 \\ 0 \end{bmatrix} = \begin{bmatrix} 0 \\ 1 \end{bmatrix} = |1\rangle \tag{2.42}$$

$$X|1\rangle = \begin{bmatrix} 0 & 1 \\ 1 & 0 \end{bmatrix} \begin{bmatrix} 0 \\ 1 \end{bmatrix} = \begin{bmatrix} 1 \\ 0 \end{bmatrix} = |0\rangle \tag{2.43}$$

Pauli X matrix is a self-adjoint matrix because when we take the adjoint of the matrix it equals the original matrix as

$$X = \begin{bmatrix} 0 & 1 \\ 1 & 0 \end{bmatrix} \rightarrow \begin{bmatrix} 0^* & 1^* \\ 1^* & 0^* \end{bmatrix} \rightarrow \begin{bmatrix} 0 & 1 \\ 1 & 0 \end{bmatrix} = X. \tag{2.44}$$

In the Bloch Sphere representation, the Pauli X operation corresponds to a rotation of π radians around the X-axis. This rotation results in a bit flip of the qubit state. If a qubit initially resides at the north pole of the Bloch Sphere, representing $|0\rangle$, the Pauli X operation will rotate it to the south pole, representing $|1\rangle$, and vice versa.

Circuit representation

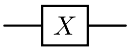

Pauli Z Operation (Z Gate): Phase Flip

The Pauli Z operation is denoted $\boldsymbol{Z}$. It is also called the phase flip operator because it leaves $|0\rangle$ unchanged and applies a phase of -1 to $|1\rangle$. The matrix representation is

$$Z = \begin{bmatrix} 1 & 0 \\ 0 & -1 \end{bmatrix}. \tag{2.45}$$

Examples of the operation

$$Z\,|0\rangle = \begin{bmatrix} 1 & 0 \\ 0 & -1 \end{bmatrix} \begin{bmatrix} 1 \\ 0 \end{bmatrix} = \begin{bmatrix} 1 \\ 0 \end{bmatrix} = |0\rangle \tag{2.46}$$

$$Z\,|1\rangle = \begin{bmatrix} 1 & 0 \\ 0 & -1 \end{bmatrix} \begin{bmatrix} 0 \\ 1 \end{bmatrix} = \begin{bmatrix} 0 \\ -1 \end{bmatrix} = -\,|1\rangle \tag{2.47}$$

Pauli Z matrix is also a self-adjoint matrix because when we take the adjoint of the matrix it equals the original matrix as

$$Z = \begin{bmatrix} 1 & 0 \\ 0 & -1 \end{bmatrix} \rightarrow \begin{bmatrix} 1^* & 0^* \\ 0^* & -1^* \end{bmatrix} \rightarrow \begin{bmatrix} 1 & 0 \\ 0 & -1 \end{bmatrix} = Z. \tag{2.48}$$

In the Bloch Sphere representation, the operation rotates the state by π over the Z-axis. Therefore, if the state was initially on the north pole, $|0\rangle$, after applying the operation nothing changes and so the state stays as $|0\rangle$. For $|1\rangle$ phase is applied so it becomes $-\,|1\rangle$. However, If a qubit initially resides at equator, representing $|+\rangle$, the Pauli Z operation will rotate it to the other side of the equator over the Z-axis, representing $|-\rangle$, and vice versa. This is becasue the Bloch sphere only represents 1 qubit system and does not represent the global phase which will be introduced later on.

Circuit representation

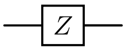

Pauli Y Operation (Y Gate): Bit-Phase Flip

The Pauli Y operation is denoted $\boldsymbol{Y}$. It is also called a bit-phase flip operator. It takes the input $|0\rangle$ to $i\,|1\rangle$ and $|1\rangle$ to $-i\,|0\rangle$. The matrix representation is

$$Y = \begin{bmatrix} 0 & -i \\ i & 0 \end{bmatrix}. \tag{2.49}$$

Examples of the operation

$$Y\,|0\rangle = \begin{bmatrix} 0 & -i \\ i & 0 \end{bmatrix} \begin{bmatrix} 1 \\ 0 \end{bmatrix} = \begin{bmatrix} 0 \\ i \end{bmatrix} = i\,|1\rangle \tag{2.50}$$

$$Y\,|1\rangle = \begin{bmatrix} 0 & -i \\ i & 0 \end{bmatrix} \begin{bmatrix} 0 \\ 1 \end{bmatrix} = \begin{bmatrix} -i \\ 0 \end{bmatrix} = -i\,|0\rangle \tag{2.51}$$

Pauli Y matrix is also a self-adjoint matrix as well since when we take the adjoint of the matrix it equals the original matrix as

$$Y = \begin{bmatrix} 0 & -i \\ i & 0 \end{bmatrix} \rightarrow \begin{bmatrix} 0 & i \\ -i & 0 \end{bmatrix} \rightarrow \begin{bmatrix} 0 & -i \\ i & 0 \end{bmatrix} = Y. \tag{2.52}$$

In the Bloch Sphere representation, the operation rotates the state by π over the Y-axis, rotation on XZ-plane. Therefore, if the state was initially on the north pole, $|0\rangle$, after applying the operation it ends up on the south pole, $|1\rangle$, and furthermore a global phase gets applied therefore becomes $i\,|1\rangle$. Similarly for $|1\rangle$, phase gets applied and rotates to the other pole so becomes $-i\,|0\rangle$. However, If a qubit initially resides at equator, representing $|i\rangle$, the Pauli Y operation will rotate it to the other side of the equator over the Y-axis, representing $|-i\rangle$, and vice versa.

Circuit representation

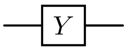

Hadamard Operation (H Gate)

The Hadamard operation, symbolized by $\boldsymbol{H}$, creates superposition of quantum states. The matrix representation is

$$H = \frac{1}{\sqrt{2}}\begin{bmatrix}1 & 1\\ 1 & -1\end{bmatrix}. \tag{2.53}$$

Examples of the operation

$$H\left|0\right\rangle = \frac{1}{\sqrt{2}}\begin{bmatrix}1 & 1\\ 1 & -1\end{bmatrix}\begin{bmatrix}1\\ 0\end{bmatrix} = \frac{1}{\sqrt{2}}\begin{bmatrix}1\\ 1\end{bmatrix} = \frac{1}{\sqrt{2}}(\left|0\right\rangle + \left|1\right\rangle) = \left|+\right\rangle \tag{2.54}$$

$$H\left|1\right\rangle = \frac{1}{\sqrt{2}}\begin{bmatrix}1 & 1\\ 1 & -1\end{bmatrix}\begin{bmatrix}0\\ 1\end{bmatrix} = \frac{1}{\sqrt{2}}\begin{bmatrix}1\\ -1\end{bmatrix} = \frac{1}{\sqrt{2}}(\left|0\right\rangle - \left|1\right\rangle) = \left|-\right\rangle \tag{2.55}$$

The states $\left|+\right\rangle$ and $\left|-\right\rangle$ represent equal superpositions, where $\left|+\right\rangle$ is an even mix of $\left|0\right\rangle$ and $\left|1\right\rangle$, and $\left|-\right\rangle$ is a similar mix but with a relative phase difference.

The Hadamard matrix is self-adjoint, meaning that it is equal to its own adjoint as

$$H = \begin{bmatrix}1 & 1\\ 1 & -1\end{bmatrix} \to \begin{bmatrix}1 & 1\\ 1 & -1\end{bmatrix} = H. \tag{2.56}$$

Circuit representation

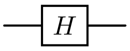

Interestingly, the Hadamard operation can be used in combination with other gates to achieve various quantum manipulations. For instance, applying the Hadamard, Z, and then Hadamard again acts as the Pauli X gate as

$$HZH = \frac{1}{\sqrt{2}}\begin{bmatrix}1 & 1\\ 1 & -1\end{bmatrix}\begin{bmatrix}1 & 0\\ 0 & -1\end{bmatrix}\frac{1}{\sqrt{2}}\begin{bmatrix}1 & 1\\ 1 & -1\end{bmatrix} = \begin{bmatrix}0 & 1\\ 1 & 0\end{bmatrix} = X. \tag{2.57}$$

Therefore, when applying it to $\left|0\right\rangle$, we can see

$$HZH\left|0\right\rangle = HZ\frac{1}{\sqrt{2}}\begin{bmatrix}1 & 1\\ 1 & -1\end{bmatrix}\begin{bmatrix}1\\ 0\end{bmatrix} = H\frac{1}{\sqrt{2}}\begin{bmatrix}1\\ -1\end{bmatrix} = \begin{bmatrix}0\\ 1\end{bmatrix} = \left|1\right\rangle, \tag{2.58}$$

flipping the state to $\left|1\right\rangle$.

Circuit representation

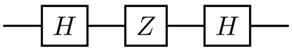

Similarly, the Hadamard operation can be used to manipulate Pauli Z gate by applying the Hadamard, X, and then Hadamard again. In matrix representation it is shown as

$$HXH = \frac{1}{\sqrt{2}}\begin{bmatrix}1 & 1\\ 1 & -1\end{bmatrix}\begin{bmatrix}0 & 1\\ 1 & 0\end{bmatrix}\frac{1}{\sqrt{2}}\begin{bmatrix}1 & 1\\ 1 & -1\end{bmatrix} = \begin{bmatrix}1 & 0\\ 0 & -1\end{bmatrix} = Z. \tag{2.59}$$

Circuit representation

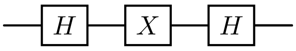

Standard Rotation Operation (Rotation Gate)

Standard rotation operations, rotate a qubit state around the Pauli axes. The rotation operation is defined as

$$R_{\hat{n}}(\theta) = e^{-i\theta\hat{n}\cdot\hat{\sigma}/2}. \tag{2.60}$$

$\hat{n}$ indicates the arbitrary axis which the state rotates in the Bloch Sphere by some arbitrary angle θ. $\hat{n}$ is a unitary vector given by coordinates, $\hat{n} = (n_x, n_y, n_z)$. $\hat{\sigma}$ is a vector given by Pauli matrices X, Y, and Z($\hat{\sigma} = (X, Y, Z)$). Therefore the equation can be decomposed into

$$e^{-i\theta\hat{n}\cdot\hat{\sigma}/2} = \cos\frac{\theta}{2}I - i\sin\frac{\theta}{2}(n_xX + n_yY + n_zZ). \tag{2.61}$$

Circuit representation for rotation around X-axis ($R_x(\theta)$), Y-axis ($R_y(\theta)$), and Z-axis ($R_z(\theta)$) are

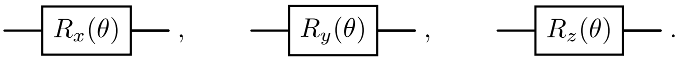

Controlled NOT Operation (CNOT Gate)

CNOT operation, sometimes called CX operation, is a quantum operation over two different qubits. One of the qubits are selected as the control or the target qubit and the operation gets applied. In particular, X operation gets applied to the state of the target qubit when the control qubit is in the $|1\rangle$ state and the X operation does not get applied when the control qubit is in the $|0\rangle$ state. For example, when the initial state is in $|\psi\rangle = |11\rangle$, the outcome is $CX|\psi\rangle = |10\rangle$ but when the $|\psi\rangle = |01\rangle$, the outcome is $CX|\psi\rangle = |01\rangle$.

The matrix representation is four-by-four matrix because it is a two-qubit operation and is described in vector notation as

$$\text{CNOT} = \begin{bmatrix} 1 & 0 & 0 & 0 \\ 0 & 1 & 0 & 0 \\ 0 & 0 & 0 & 1 \\ 0 & 0 & 1 & 0 \end{bmatrix}. \tag{2.62}$$

The CNOT operation can be represented using Bra-ket notation as

$$\text{CNOT} = |0\rangle\langle 0| \otimes I + |1\rangle\langle 1| \otimes X, \tag{2.63}$$

where $|0\rangle\langle 0|$ and $|1\rangle\langle 1|$ are projectors on the control qubit, and I and X are the operations on the target qubit.

Circuit representation

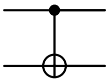

For multiple-qubit gates, the black dot is the control qubit and whatever the symbol is on the other end of the vertical line is the target qubit.

Controlled Z Operation (CZ Gate)

CZ operation, similarly to the CNOT operation is an operation over two different qubits. Z operation gets applied to the state of the target qubit when the control qubit is in the $|1\rangle$ state and the Z operation does not get applied when the control qubit is in the $|0\rangle$ state. For example, when the initial state is in $|\psi\rangle = |11\rangle$, the outcome is $CZ|\psi\rangle = -|11\rangle$ but when the $|\psi\rangle = |01\rangle$, the outcome is $CZ|\psi\rangle = |01\rangle$. The matrix representation for CZ operation is

$$CZ = \begin{bmatrix} 1 & 0 & 0 & 0 \\ 0 & 1 & 0 & 0 \\ 0 & 0 & 1 & 0 \\ 0 & 0 & 0 & -1 \end{bmatrix}. \tag{2.64}$$

The CZ operation can be represented using Bra-ket notation as

$$\text{CZ} = |0\rangle\langle 0| \otimes I + |1\rangle\langle 1| \otimes Z, \tag{2.65}$$

where $|0\rangle\langle 0|$ and $|1\rangle\langle 1|$ are projectors on the control qubit, and I and Z are the operations on the target qubit.

Circuit representation

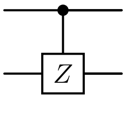

Since $HXH = Z$, it allows us to transform a CX circuit into CZ) gate. We apply Hadamard gates before and after the target qubit of the CX gate. circuit representation is

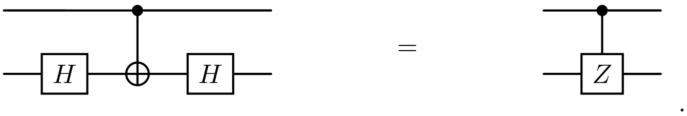

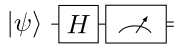

Figure 2.4: Measurement in Pauli X basis using Pauli Z measurement

2.2.5 Measurement in Quantum Computing

Measurement is the operation which we extract the classical information from the qubit. Remember, qubits can be in superposition of multiple states, however when we measure them, the state collapses to one of them. In analogy, the coin has the possibility of being heads or tail while it is in air, but it is measured as only heads or tail, when landed.

This measurement process can be explained in more detail mathematically. In a quantum system such as qubit state, observables are represented by Hermitian operators. Observables are physical quantity that are measurable. For example, Pauli Z, Pauli X, Pauli Y matrices are observables and are Hermitian operators as explained in their section. Intuitively, when the qubits go through the detector, we are asking about their classical states in the observables, asking what they are in the basis of the observables such as the Pauli Z basis. Then the detector will give us the measurement outcome which is the eigenvalue such as +1 or -1 which corresponds to the observables. This is possible because for a quantum system, the eigenstate is associated with its eigenvalue and the observables. When σ_B is the observable, ψ_n is the eigenstate, and e_n is the eigenvalue, the relation could be expressed in equation as

$$\sigma_B \psi_n = e_n \psi_n. \tag{2.66}$$

For example, when we have Pauli Z matrix as the observable, the eigenstate would be $|0\rangle$ or $|1\rangle$ and the corresponding eigenvalue would be +1 or -1. I described the measurement process mathematically in general quantum mechanics.

For quantum computation, we use projection operators denoted $\Pi_{\pm}^{B}$ as the observables. Projection operators are outerproduct of certain state in certain basis. B represents the certain basis such as Pauli Z, X, and Y. ± describes the eigenstate of the operator. It is also important to understand that these state vectors are orthogonal as well. Therefore, projection operator can be described as

$$\Pi_{\pm}^{B} = |b_{\pm}\rangle\langle b_{\pm}| \tag{2.67}$$

Example of $|b_{\pm}\rangle\langle b_{\pm}|$ will be $|0\rangle\langle 0|$ and $|1\rangle\langle 1|$ when the observable is the Pauli Z matrix, $|+\rangle\langle +|$ and $|-\rangle\langle -|$ when the observable is the Pauli X matrix, and $|i\rangle\langle i|$ and $|-i\rangle\langle -i|$ when the observable is the Pauli Y matrix.

When we are given a specific state that we want to measure $|\psi\rangle$, the probability, $p(b)$, of measuring that state in certain observable can be obtained by

$$p(b) = |\langle \Pi_{\pm}^{B} | \psi \rangle|^2. \tag{2.68}$$

Typically, a measurement device yields a binary outcome, commonly represented by the values 0 and 1. The likelihood of each outcome is determined by the above equation which was actually asking what the eigenvalue of the state is when the system collapses to one of the eigenstate of the observable. This post-measurement state, ϕ_b, can be expressed as

$$|\phi_b\rangle = \frac{\Pi_{\pm}^{B}|\psi\rangle}{\sqrt{p(b)}}. \tag{2.69}$$

As shown in Figure 2.4, measurement in the Pauli X basis can be done by applying an Hadamard gate before performing a standard Pauli Z basis measurement. Measurements in other bases, such as the Y Pauli basis follow similar procedures.

2.2.6 Probability and Expectation Value

Now that we discussed measurement for a single quantum system, let's consider a scenario where we have multiple copies of the same quantum state $|\psi\rangle$ that satisfy equation 2.1. By measuring these states repeatedly, we can gather statistical information about the outcome probabilities. Suppose we perform a series of measurements on these qubits. We would then obtain a sequence of outcomes, represented by a string of +1s and -1s. The ratio of the number of +1 outcomes to the total number of measurements gives an approximation of the probability of observing a +1 outcome as

$$Prob\{+1\} = \frac{N(+1)}{N(+1) + N(-1)} \approx |\alpha|^2. \tag{2.70}$$

Similarly, for -1 outcomes we can say

$$Prob\{-1\} = \frac{N(-1)}{N(+1) + N(-1)} \approx |\beta|^2. \tag{2.71}$$

Although the outcomes of individual measurements are random, the expected value, or mean result, can be calculated similarly to classical expectation values. For example, the expectation value when measuring in the Pauli Z basis is computed as

$$\mathbb{E}[Z] = Prob(+1) \cdot (+1) + Prob(-1) \cdot (-1) = |\alpha|^2 - |\beta|^2. \tag{2.72}$$

In Dirac notation, this expectation value is expressed as

$$\begin{aligned} \langle Z \rangle &= \langle \psi | Z | \psi \rangle & (2.73)\\ &= \begin{bmatrix} \alpha^* & \beta^* \end{bmatrix} \begin{bmatrix} 1 & 0 \\ 0 & -1 \end{bmatrix} \begin{bmatrix} \alpha \\ \beta \end{bmatrix} & (2.74)\\ &= \begin{bmatrix} \alpha^* & \beta^* \end{bmatrix} \begin{bmatrix} \alpha \\ -\beta \end{bmatrix} & (2.75)\\ &= |\alpha|^2 - |\beta|^2. & (2.76) \end{aligned}$$

The randomness of the measurement outcomes introduces some variance, which can be computed using classical probability theory as

$$Var[Z] = \mathbb{E}[Z^2] - (\mathbb{E}[Z])^2. \tag{2.77}$$

The term $\mathbb{E}[Z^2]$ is given by

$$\mathbb{E}[Z^2] = Prob\{+1\} \cdot (+1)^2 + Prob\{-1\} \cdot (-1)^2 = |\alpha|^2 + |\beta|^2. \tag{2.78}$$

The squared expectation value $\mathbb{E}[Z]^2$ is simply the square of $\mathbb{E}[Z]$. Thus, the variance of Z, often referred to as the fluctuation in physics, can be expressed in Dirac notation as

$$(\Delta Z)^2 \equiv Var[Z] = \langle Z^2 \rangle - \langle Z \rangle^2. \tag{2.79}$$

2.2.7 Entanglement

Entanglement is an essential quantum phenomenon. Phenomenon in which illustrates strong correlations between two or more quantum systems. This phenomenon has no classical analogue, making it unique. Entangled states are defined as global states that cannot be decomposed into a tensor product of individual local states. This suggests that while we may possess complete knowledge of the combined state of the system, the state of each individual component remains unknown.

For example, consider a scenario where we are given a global entangled state $|\psi\rangle_{AB} = \frac{1}{\sqrt{2}}(|00\rangle + |11\rangle)$. The general states of qubit A and B can be expressed as equation 2.30. We can attempt to represent the global state as a tensor product of these individual states as equation 2.31. By comparing the global state $|\psi\rangle_{AB}$ with the tensor product of $|\psi\rangle_A$ and $|\psi\rangle_B$, we find that the coefficients must satisfy the following conditions;

$$a_0 b_0 = a_1 b_1 = \frac{1}{\sqrt{2}}, \qquad a_0 b_1 = a_1 b_0 = 0. \tag{2.80}$$

However, to satisfy these conditions, either a_0 or b_1 must be zero, which contradicts the requirement that $a_0 b_0 = a_1 b_1 = \frac{1}{\sqrt{2}}$. This contradiction reveals that the state $|\psi\rangle_{AB}$ cannot be represented as a tensor product of individual local states, therefore, illustrating the inherent entanglement of the global state. Notice that in the Product State section, we were able to obtain the local states from the global states. Entangled states, by definition does not allow us to do that.

Bell State

Bell states are examples of two-qubit entangled states that are used commonly in quantum fields. There are four of them and are written in the Dirac notation as

$$|\Phi^+\rangle = \frac{1}{\sqrt{2}}(|00\rangle + |11\rangle), \tag{2.81}$$

$$|\Phi^-\rangle = \frac{1}{\sqrt{2}}(|00\rangle - |11\rangle), \tag{2.82}$$

$$|\Psi^+\rangle = \frac{1}{\sqrt{2}}(|01\rangle + |10\rangle), \tag{2.83}$$

$$|\Psi^-\rangle = \frac{1}{\sqrt{2}}(|01\rangle - |10\rangle). \tag{2.84}$$

To describe each bipartite Bell pair, we have to consider the pure and mixed states. Pure states are states when we have full knowledge of the states and the mixed states is when we do not have the perfect knowledge of the states, when there are uncertainties. In the case of real world scenarios, we always have to consider the noise with uncertainty which is the mixed states. In terms of notation, for mixed states we use the ρ symbol, and can only be expressed by matrices, often called the density matrix. For pure states we use ket symbols such as $|\psi\rangle$ and can be represented by vectors and matrices. To normalize the mixed states you have to satisfy the trace of the density matrix as $Tr\{\rho\} = 1$. For pure state the normalization condition is $|\langle\psi|\psi\rangle|^2 = 1$. The difference between the pure state and mixed states are clear when we consider two specific example, an equal superposition and a maximally mixed state. An equal superposition will be expressed as

$$|\psi\rangle = \frac{1}{\sqrt{2}}|0\rangle + \frac{1}{\sqrt{2}}|1\rangle. \tag{2.85}$$

and density matrix of a maximally mixed state could be expressed as

$$\rho = \frac{1}{2}|0\rangle\langle 0| + \frac{1}{2}|1\rangle\langle 1| = \frac{1}{2}\begin{bmatrix}1 & 0\\ 0 & 0\end{bmatrix} + \frac{1}{2}\begin{bmatrix}0 & 0\\ 0 & 1\end{bmatrix} = \frac{1}{2}\begin{bmatrix}1 & 0\\ 0 & 1\end{bmatrix}. \tag{2.86}$$

In the Bloch Sphere notation, the maximally mixed state means a state placed in the center of the sphere, furthest away from the surface of the sphere is where the pure states will be placed, also meaning that we have the most uncertain state. They both look intuitively similar. In fact when we measure them both in the Pauli Z basis, we get

$$Prob\{+1\}_{\text{pure state}} = \frac{1}{2}(\text{in state}\,|0\rangle), \quad Prob\{-1\}_{\text{pure state}} = \frac{1}{2}(\text{in state}\,|1\rangle), \tag{2.87}$$

$$Prob\{+1\}_{\text{mixed state}} = \frac{1}{2}(\text{in state}\,|0\rangle), \quad Prob\{-1\}_{\text{mixed state}} = \frac{1}{2}(\text{in state}\,|1\rangle). \tag{2.88}$$

However when we rotate the measurement basis from Z basis to X basis, we can see the difference. We can rewrite each states in the Pauli X basis as

$$|\psi\rangle = \frac{1}{\sqrt{2}}|0\rangle + \frac{1}{\sqrt{2}}|1\rangle = |+\rangle, \tag{2.89}$$

$$\rho = \frac{1}{2}|0\rangle\langle 0| + \frac{1}{2}|1\rangle\langle 1| = \frac{1}{2}|+\rangle\langle +| + \frac{1}{2}|-\rangle\langle -|. \tag{2.90}$$

When we look at the probabilities of different measurement outcomes we get

$$Prob\{+1\}_{\text{pure state}} = 1(\text{in state}\,|+\rangle), \quad Prob\{-1\}_{\text{pure state}} = 0(\text{in state}\,|-\rangle), \tag{2.91}$$

for the pure state, and

$$Prob\{+1\}_{\text{mixed state}} = \frac{1}{2}(\text{in state}\,|+\rangle), \quad Prob\{-1\}_{\text{mixed state}} = \frac{1}{2}(\text{in state}\,|-\rangle), \tag{2.92}$$

for maximally mixed state. For the pure state you can notice that we will never get the measurement outcome of {-1} because the initial state has no $|-\rangle$ component. Where as the ρ of the maximally mixed state can still be found in the $|+\rangle$ and $|-\rangle$ 50% of the times. To see the difference between these two states we need to measure and check them in different basis.

Going back to the description of bipartite Bell pair, given a bipartite Bell pair A and B, if we measure one of the qubit, the outcomes are uniformly random for any basis. For example when we have a $|\Phi^+\rangle = \frac{1}{\sqrt{2}}(|00\rangle + |11\rangle$ and we only measure qubit A, the probability outcome for each basis are

$$\text{Pauli Z basis, Pauli X basis, Pauli Y basis} : Prob\{+1\} = Prob\{-1\} = \frac{1}{2}, \tag{2.93}$$

Same thing could be said for when measuring qubit B. No matter which basis we measure in, we get 50% +1 out come and 50% -1 outcome. This is because the state is maximally entangled. The correct description of the local qubits must be given in terms of density matrices as state of qubit A and qubit B could be described as

$$\rho_A = \frac{1}{2}(|0\rangle\langle 0| + |1\rangle\langle 1|), \tag{2.94}$$

$$\rho_B = \frac{1}{2}(|0\rangle\langle 0| + |1\rangle\langle 1|). \tag{2.95}$$

Bell state measurement

The four Bell states (equations 2.81, 2.82, 2.83, 2.84) are orthonormal basis which means if you take the inner product of the same Bell state you will get 1 and if you take the inner product of two different Bell state you will get 0 as

$$\langle\Phi^+|\Phi^+\rangle = 1, \qquad \langle\Phi^-|\Psi^+\rangle = 0. \tag{2.96}$$

Therefore, we can rewrite Pauli Z basis in terms of the Bell basis. The following are examples of rewriting the two-qubit states in the Bell basis.

$$|00\rangle = \frac{1}{\sqrt{2}}(|\Phi^+\rangle + |\Phi^-\rangle), \tag{2.97}$$

$$|01\rangle = \frac{1}{\sqrt{2}}(|\Psi^+\rangle + |\Psi^-\rangle), \tag{2.98}$$

$$|10\rangle = \frac{1}{\sqrt{2}}(|\Psi^+\rangle - |\Psi^-\rangle), \tag{2.99}$$

$$|11\rangle = \frac{1}{\sqrt{2}}(|\Phi^+\rangle - |\Phi^-\rangle). \tag{2.100}$$

This implies that any pure state of two-qubit $|\psi\rangle = \alpha\,|00\rangle + \beta\,|01\rangle + \gamma\,|10\rangle + \delta\,|11\rangle$ can be written in Bell basis as

$$|\psi\rangle = \frac{\alpha+\beta}{\sqrt{2}}\,|\Phi^+\rangle + \frac{\alpha-\beta}{\sqrt{2}}\,|\Phi^-\rangle + \frac{\gamma+\delta}{\sqrt{2}}\,|\Psi^+\rangle + \frac{\gamma-\delta}{\sqrt{2}}\,|\Psi^-\rangle\,. \tag{2.101}$$

Now, we can measure in Bell basis and know the probabilities of the various outcomes we get. Four measurement outcomes and the probabilities of measuring each Bell states could be written as

$$Prob|\Phi^+\rangle = \frac{|\alpha+\beta|^2}{2}, \tag{2.102}$$

$$Prob|\Phi^-\rangle = \frac{|\alpha-\beta|^2}{2}, \tag{2.103}$$

$$Prob|\Psi^+\rangle = \frac{|\gamma+\delta|^2}{2}, \tag{2.104}$$

$$Prob|\Psi^-\rangle = \frac{|\gamma-\delta|^2}{2}. \tag{2.105}$$

To do the Bell state measurement using only the Pauli Z measurement, we need CNOT gate and Hadamard gate before we measure the state, similar to how single qubit X basis measurement was done, using the Z basis measurement. We want to find the unitary that will satisfy

$$U\,|\Phi^+\rangle = |00\rangle\,, \tag{2.106}$$

$$U\,|\Phi^-\rangle = |10\rangle\,, \tag{2.107}$$

$$U\,|\Psi^+\rangle = |01\rangle\,, \tag{2.108}$$

$$U\,|\Psi^-\rangle = |11\rangle\,. \tag{2.109}$$

The circuit in figure 2.5 satisfies the above condition.

This tells us that if we get the outcome of 00 which corresponds to +1+1, we know that we have the Bell state $|\Phi^+\rangle$. Similary for the all the other three measurement outcomes, we know that if we get; 01 we have $|\Psi^+\rangle$, 10 we have $|\Phi^-\rangle$, 11 we have $|\Psi^-\rangle$.

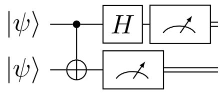

Figure 2.5: Circuit for finding the U for Bell State measurement in Z basis

2.2.8 Quantum Teleportation

Quantum teleportation allows the transmission of quantum information, encapsulated in a quantum state, without requiring the physical movement of the system encoding this message [4]. This process is quite amazing in the context of quantum communication, where information can be transmitted without the direct transfer of the physical system itself.

Consider a scenario involving two participants: Alice and Bob. In this setup, Alice's goal is to send a quantum state, denoted as $|\psi\rangle = \alpha|0\rangle + \beta|1\rangle$, to Bob. Alice possesses an arbitrary qubit $|\psi\rangle$, while both Alice and Bob share an entangled state, represented by $|\Phi^+\rangle = \frac{1}{\sqrt{2}}(|00\rangle + |11\rangle)$. The total composite system, Alice's qubit and the shared entangled pair, can be expressed as

$$|\psi\rangle_{\text{total}} = |\psi\rangle_A \otimes |\Phi^+\rangle_{AB} = \frac{1}{\sqrt{2}}(\alpha|000\rangle + \alpha|011\rangle + \beta|100\rangle + \beta|111\rangle). \tag{2.110}$$

In the process of quantum teleportation, Alice carries out a measurement in the Bell basis on her set of qubits. This measurement results in one of four possible outcomes, each corresponding to a distinct Bell state. The outcome of this measurement is then relayed to Bob via a classical communication channel. It is important to note that the probability of obtaining each of the four possible Bell states as a result of Alice's measurement is equally likely, with a probability of $\frac{1}{4}$. After receiving the classical measurement outcome, Bob then applies a specific unitary operation to his qubit. The choice of this operation is dependent on the particular Bell state measured by Alice.

- If Alice's measurement is $|\Phi^+\rangle$, Bob applies nothing, the I gate.
- If Alice's measurement is $|\Phi^-\rangle$, Bob applies the Z gate.
- If Alice's measurement is $|\Psi^+\rangle$, Bob applies the X gate.
- If Alice's measurement is $|\Psi^-\rangle$, Bob applies the ZX gate.

By following the protocol and applying the appropriate unitary operation based on Alice's communicated measurement result, Bob successfully reconstructs the state $|\phi\rangle$ on his qubit. It is important note that this protocol requires the classical communication between Alice and Bob and a shared Entangled Bell pair between them. Figure 2.3 shows the circuit diagram of the protocol.

2.2.9 Promised Quantum Advantages

After exploring the basics of quantum information, it is clear why there are excitements about quantum computing. For certain problems, it is assumed that quantum computer could be faster and more powerful than classical computers. Google claimed they achieved such advantage with their quantum computer, calling it quantum supremacy [1]. There is also progress in the field of quantum chemistry. In 2016, researchers used a quantum computer to figure out the energy of a hydrogen molecule [37, 26]. This is just one example of how quantum computing can solve complex real-world problems.

However, today's quantum computers, known as Noisy Intermediate-Scale Quantum (NISQ) devices [40], are still at early-stage of the useful hardware, with challenges such as the number of qubits and substantial amount of errors. With a Fault-Tolerant Quantum Computer and techniques like quantum error correction, we can see the potential of running algorithms like Shor's [44, 18] and Grover's [20]. These algorithms offer faster solutions than classical ones. Looking forward, there are several propositions for more breakthroughs. Tools like the Variational Quantum Eigensolver [39, 34] and the Quantum Approximate Optimization Algorithm [14] are showing great potential for algorithm and optimization.

In any matter, to scale the computation, we either have to think of a larger processor or a construction of a quantum network. However, to manipulate millions of qubits and ideal gates, large processor is not realistic as I will mention in the Actual Device section. Therefore, building the quantum network to scale the quantum computation is inevitable not only for the advantages mentioned above but for some unique usage as well.

2.3 Quantum Network

Quantum networks is a network that enables the transmission of quantum information and various applications that are not possible in the classical network. In quantum networks, nodes which could be individual qubits or clusters of qubits, are interconnected not just physically but through the phenomenon of quantum entanglement. We use entanglement system as the link of the nodes which I will be referring to as entangled link.

Important example of quantum networking in action we have already looked at is quantum teleportation [4]. Unlike classical networking, where information is physically transmitted across connections, quantum teleportation relies on entanglement and measurement. When a sender node (Alice) performs a measurement in the process of teleportation, the entangled link between the nodes is consumed, and simultaneously, the quantum information is propagated to the next node. This consumption of entanglement, known as link-level entanglement, is unique to quantum networks. Each operation within these networks can decrease the network's accuracy or integrity of the quantum information being transmitted. As operations are performed, entangled link can degrade. Therefore, in quantum networks, maintaining and distributing useful entanglement is important.

2.3.1 Application and Significance

There are three big applications of quantum networks that are thought to be significant. For instance, as mentioned in the Promised Quantum Advantages section, scaling of quantum computer is an important problem to tackle. The approach of connecting multiple quantum computer, is thought to be one solution. Implementation of Shor's algorithm is a cornerstone in quantum computing known for its potential to factor large numbers. This would require about 20 million noisy qubits to factor a 2048-bit RSA encryption [18]. There have been a paper showing feasible implementation of Shor's algorithm using distributed quantum computer [35]. If we can successfully scale quantum computers, other advantages mentioned in the Promised Quantum Advantages section could also be achieved as well.

Quantum networks will also have crucial impact in the domain of security. In classical communication systems, encryption is employed to guard messages, but current cryptosystems remain vulnerable to decryption, especially with the advent of fault-tolerant quantum computers in the future. Quantum computers, in this sense, are double-edged swords: posing a threat to existing encryption methods but also holding the key to new levels of security. This dichotomy is particularly evident in entanglement-based quantum key distribution (QKD). QKD enables the secure transfer of classical information through a public quantum channel, significantly strengthening security against eavesdropping by detecting the eavesdropper [13]. There have already been a successful demonstration of a QKD operation which showed successful video transmisson over the distance of 45km, detecting the eavesdropper in 2010 in Japan [43]. QKD experiment was also practically demonstrated in an experiment where researchers successfully achieved QKD between a satellite and ground stations [32].

Another promising application of quantum networks lies in the realm of quantum sensoring networks. These networks can significantly enhance sensitivity, a development with substantial implications for quantum metrology [19], using the multi-entangled state, the GHZ state. It will increase the visibility of satellites. The heightened sensitivity of quantum sensoring networks could lead to advancements in various fields, from environmental monitoring to precision navigation.

Chapter 3

Problem Statement and Proposal

As mentioned, in quantum networks, maintaining and distributing "useful" entanglement is important. Take entanglement-based QKD for example, Alice and Bob has to share a maximally entangled state in order to produce a partially correlated key. Better quality of entangled state will create stronger security when establishing a secret key. However within the entangled link, there exists various types of noises that degrade the quality of the entangled link. One traditional way of knowing how the link was affected by the noises, is by performing the state tomography. However this requires the measurement of the entangled Bell Pair in use, which stops the application from being used. Furthermore, this traditional approach is not efficient as it requires relatively big amount of resources. Maity et al in OIST, have came up with new approach to tackle this problem. However, this approach has never been tested on actual device. I address two problems to be tackled. One of the problem being, the traditional approach of characterizing Pauli errors in entangled link is inefficient and requires stopping the application. Another being, the new approach by Maity et al to tackle the first problem have never been tested on actual quantum device. In this chapter, I will explain terms such as entangled link, noise, Pauli errors, fidelity, state tomography, and purification, to understand the problem statement and approaches to solve them, more in detail.

3.1 Entangled Link

In quantum network, as mentioned several times, entangled link is used. For simplicity, in my project, I used the $|\Phi^+\rangle$ Bell state as the simulated link. In the density form, this entangled link can be written as

$$\rho = |\Phi^+\rangle \langle\Phi^+| . \tag{3.1}$$

In the circuit representation, this link could be simulated, as shown in figure 3.1.

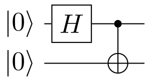

Figure 3.1: Circuit for creating a $|\Phi^+\rangle$ Bell pair

3.2 Noisy world

So far, I have only explained quantum states which was noiseless. So the states were always in the state which we intended it to be and we had full knowledge of the state as well. However in the real world, there are unwanted noises.

There are two classes of noise in quantum communication which are loss error and operational error. Loss error is caused by attenuation of photons in the fiber and free space. Even before going through the fiber, there is the coupling inefficiency, where the photon generated by the source have problems being captured to travel through the fiber. Furthermore, the detector could also have inefficiencies to detect the photon. The rate of communication due to loss error, decreases exponentially with distance.

Operational error include measurement error, local gate error, memory decoherence, and channel decoherence. Measurement error is also called the read out error which are errors that occur in the measurement process. The measurement outcome could differ from the actual state of the qubit. Local gate errors occur when you try to operate your qubit inside the memory. The other three error could have coherent and incoherent errors.

Coherent error happens deterministically, often unitary, so it is easier to correct. For example, if you can generate the same Bell pair with a specific state. Once you are able to characterize that state, you just have to calibrate the hardware every time in same manners.

Incoherent errors occur stochastic-ally. It could be both unitary operation (Pauli error) which will be explained in the next section, or non-unitary such as the relaxation channel. Within the types of unitary channel, the phase flip channel, is also called the de-phasing channel because when there is a strong application of the phase flip error, the information about the relative phase of the quantum system can be washed away. The relaxation channel(amplitude damping channel) ρ_r of a single quantum system is described as

$$\rho_r = K_0 \rho {K_0}^\dagger + K_1 \rho {K_1}^\dagger. \tag{3.2}$$

The K_0 and K_1 are called the Kraus operator which is described as

$$K_0 = \begin{pmatrix} 1 & 0 \\ 0 & \sqrt{1-\gamma}, \end{pmatrix} \tag{3.3}$$

$$K_1 = \begin{pmatrix} 0 & \sqrt{\gamma} \\ 0 & 0 \end{pmatrix}. \tag{3.4}$$

where γ is the probability of the relaxation strength applied. When the γ is high, the pure state on any surface of the Bloch sphere gets squashed towards the north pole which represent $|0\rangle$.

Dephasing and relaxation noise are also called the decoherent noise which are caused by its external environment [29]. Specifically, external environment such as electromagnetic noise, interactions with nearby particles, and thermal fluctuations, cause the decoherent noise. Thermal fluctuations can impact two important time constants [45]: T_1 (thermal relaxation time) and T_2 (dephasing time). T_1 time, characterizes the time it takes for a qubit to lose its energy to the environment often referred to as the time for amplitude damping in the relaxation channel. When the state gets squashed towards, $|0\rangle$, is actually losing its energy. T_2 represents how quickly a qubit loses its phase information referred to as the phase damping in the phase flip channel. Even when you do not manipulate the qubit and just store it inside a memory, it decoheres. such error is called the memory decoherence. In this project, my goal is to characterize the Pauli errors which are incoherent error.

3.2.1 Pauli Errors

Pauli errors are unwanted Pauli gate rotation that gets introduced to the channel or link. For example, assume the case where we have a channel that want to send the ideal state, $|\psi\rangle$. Against our will, the state under goes a Pauli X operation. Such channel could be referred to as the bit flip channel. The density matrix could be used to describe the channel. Consider the scenario where the actual output that got sent was $X|\psi\rangle$. When the bit flip error occur with the probability of p_x, the output could be written in the density matrix form as

$$\rho = (1-p_x)|\psi\rangle\langle\psi| + p_x X|\psi\rangle\langle\psi| X. \tag{3.5}$$

Similarly, the output for Pauli Z error (Phase flip) channel could be written as

$$\rho = (1-p_z)|\psi\rangle\langle\psi| + p_z Z|\psi\rangle\langle\psi| Z. \tag{3.6}$$

Similary, the output for the Pauli Y error (Bit phase flip) channel could be described as

$$\rho = (1-p_y)|\psi\rangle\langle\psi| + p_y Y|\psi\rangle\langle\psi| Y. \tag{3.7}$$

When $|\Phi^+\rangle$, an entangled simulated Bell state undergoes a bit flip channel, the output can be described as

$$\rho = (1-p_x)|\Phi^+\rangle\langle\Phi^+| + p_x X|\Phi^+\rangle\langle\Phi^+| X. \tag{3.8}$$

We will get $|\Phi^+\rangle$ with probability of $(1-p_x)$, and $X|\Phi^+\rangle = |\Psi^+\rangle$ with probability of p_x. Similarly, for a phase flip channel, the output can be described as

$$\rho = (1-p_z)|\Phi^+\rangle\langle\Phi^+| + p_z Z|\Phi^+\rangle\langle\Phi^+| Z. \tag{3.9}$$

We will get $|\Phi^+\rangle$ with probability of $(1-p_z)$, and $Z|\Phi^+\rangle = |\Phi^-\rangle$ with probability of p_z.Same for bit phase flip channel, the output can be described as

$$\rho = (1-p_y)|\Phi^+\rangle\langle\Phi^+| + p_y Y|\Phi^+\rangle\langle\Phi^+|Y. \tag{3.10}$$

We will get $|\Phi^+\rangle$ with probability of $(1-p_y)$, and $X|\Phi^+\rangle = |\Psi^-\rangle$ with probability of p_y. My goal of this project is to characterize, with how much probability, each of these three Pauli errors occur in the entangled simulated link. For simplicity, in this project we used a certain assumption called the werner assumption which will be explained later in the section of Werner state.

3.2.2 Fidelity

To measure the quality of the entangled link, we use the fidelity. Fidelity in definition, is a metric that compares the distance between two quantum states [31]. The fidelity F for two quantum states ρ and σ is defined as

$$F(\rho,\sigma) = tr\sqrt{\sqrt{\rho}\sigma\sqrt{\rho}}. \tag{3.11}$$

tr is the trace of the computed matrix. In the context of my project, it could be used to compare the two states; the actual output state that went through the noisy channel and the ideal output state intended to go through the channel. In other words, fidelity could be used to describe the quality of the output we get. Thus, fidelity is used as one of the verification methods [48]. When ρ is the actual mixed output state and $|\psi\rangle$ is the desired output it could be written as

$$F(\rho,|\psi\rangle) = \langle\psi|\rho|\psi\rangle. \tag{3.12}$$

This shows that the fidelity is actually the expectation value of the density matrix ρ with respect to the pure state $|\psi\rangle$. Fidelity varies between 0 and 1, shown as

$$0 \leq F(\rho,|\psi\rangle) \leq 1. \tag{3.13}$$

When the fidelity is 0, the actual output is orthogonal to the desired output. This means the actual output could be completely distinguishable from the desired output, meaning the quality of the output is low in respect to the desired output. When the fidelity is 1 it means the desired output and the actual output is the same. For example, consider the case when the output is the completely desired state. The actual output could be written as a density matrix as

$$\rho = |\psi\rangle\langle\psi|. \tag{3.14}$$

Substituting it to the equation 3.12, we can get

$$F(\rho,|\psi\rangle) = \langle\psi|\psi\rangle^2 = 1. \tag{3.15}$$

Similarly, obtaining the fidelity of the actual Bell state output ρ that went a bit flip channel, from equation 3.8, and a desired Bell state $|\Phi^+\rangle$, could be done by calculating

$$F(\rho,|\Phi^+\rangle) = \langle\Phi^+|\rho|\Phi^+\rangle. \tag{3.16}$$

When there is no error at all, we will get $\rho = |\Phi^+\rangle\langle\Phi^+|$, and by substituting this to equation 3.13, we get

$$F(\rho,|\Phi^+\rangle) = \langle\Phi^+|\rho|\Phi^+\rangle = \langle\Phi^+|\Phi^+\rangle^2 = 1. \tag{3.17}$$

If the state undergoes a bit flip error, we will get an orthogonal state, $\rho = |\Psi^+\rangle\langle\Psi^+|$, and again by substituting this to equation 3.13, the fidelity could be computed as

$$F(\rho,|\Phi^+\rangle) = \langle\Phi^+|\rho|\Phi^+\rangle = \langle\Psi^+|\Phi^+\rangle^2 = 0. \tag{3.18}$$

Here, we have to note that the state is entangled, even though we do not have the desired entangled state.

Now, consider the scenario when the output is maximally mixed and we want to prepare the state$|\psi\rangle = |0\rangle$. The output could be written as

$$\rho = \frac{1}{2}|0\rangle\langle 0| + \frac{1}{2}|1\rangle\langle 1|. \tag{3.19}$$

Substituting it to the equation 3.12, we get

$$F(\rho, |\psi\rangle) = \langle 0| \rho |0\rangle \tag{3.20}$$

$$= \frac{1}{2}\langle 0|0\rangle + \frac{1}{2}\langle 0|1\rangle^2 \tag{3.21}$$

$$= \frac{1}{2}. \tag{3.22}$$

For two-qubit, consider the case where we want to prepare two initial state $|00\rangle$, and the output is maximally mixed. The condition could be written as

$$\rho = \frac{1}{4}(|00\rangle\langle 00| + |01\rangle\langle 01| + |10\rangle\langle 10| + |11\rangle\langle 11|), \tag{3.23}$$

$$|\psi\rangle = |00\rangle. \tag{3.24}$$

By substituting it to equation 3.12, we can get

$$F(\rho, |\psi\rangle) = \langle 00| \rho |00\rangle = \frac{1}{4}. \tag{3.25}$$

This could be generalized, that for N qubits, if we are trying to initialize them in a $|0\rangle$ state, and our actual output was a maximally mixed state of N qubits, the fidelity scale as

$$F(\rho, |\psi\rangle) = \frac{1}{2^N}. \tag{3.26}$$

Using the equation 3.12, the fidelity of a bit flip error channel with the desired output state $|0\rangle$ could be computed as

$$F(\rho, |0\rangle) = \langle 0| \rho |0\rangle \tag{3.27}$$

$$= (1-p)\langle 0|0\rangle^2 + p|\langle 0|1\rangle|^2 \tag{3.28}$$

$$= 1 - p. \tag{3.29}$$

This shows that the error probability has effect on the fidelity. Using this relation, the output description of entangled state that underwent a bit flip error from equation 3.8 could be rewritten as

$$\rho = F|\Phi^+\rangle\langle\Phi^+| + (1-F)|\Psi^+\rangle\langle\Psi^+|. \tag{3.30}$$

Again, this shows that the characterization of the errors are important as it determines the quality of the system.

Fidelity could be interpreted that the output we actually have, passed a test for being the desired output state. Fidelity less than 1 does not mean it is a completely useless state. We can use it as long as it satisfies the requirement, often being higher than certain criterion, for each protocol, written as

$$F(\rho, |\psi\rangle) > F_{crit}. \tag{3.31}$$

The main purpose of my project is to estimate how much these fidelity or error probabilities for each Pauli errors. There is already an approach to actually know about these error probability which I will introduce in the next section.

3.3 Traditional Approach: Performing State Tomography

The traditional approach of knowing about the errors in the channel [8] is by performing state tomography [10]. We construct the information of the whole system by doing different type of measurement, multiple times. This allows us to know the state of an unknown physical quantum system. Specifically, we try to obtain the elements of a following physical quantum system ρ. Any single-qubit state can be written as

$$\rho = \frac{1}{2}(I + \overrightarrow{r} \cdot \overrightarrow{\sigma}) = \begin{bmatrix} 1 + r_z & r_x - ir_y \\ r_x + ir_y & 1 - r_z \end{bmatrix}, \tag{3.32}$$

when given

$$\rho = \begin{bmatrix} \rho_{00} & \rho_{01} \\ \rho_{10} & \rho_{11} \end{bmatrix}. \tag{3.33}$$

$\overrightarrow{r}$represents the Bloch vector. These the expectation values of each operator in the Pauli basis. Geometrically, on the Bloch Sphere, it is the number described to show how much it is from the center and could be described as

$$\overrightarrow{r} = (r_x, r_y, r_z) \tag{3.34}$$

$\overrightarrow{\sigma}$ represents the Pauli vectors as

$$\overrightarrow{\sigma} = (X, Y, Z) \tag{3.35}$$

To know the diagonal elements, ρ_{00} and ρ_{11}, we only need the r_z components. To know the off-diagonal components, ρ_{01} and ρ_{10}, we need the r_x and r_y components. To know the Bloch vector components, we measure the expectation values of the Pauli operators. For example the expectation values for the Pauli X operator can be computed as

$$\begin{aligned}
\langle X \rangle &= Tr\{X_\rho\} && (3.36)\\
&= Tr\{X\frac{1}{2}(I + r_xX + r_yY + r_zZ)\} && (3.37)\\
&= \frac{1}{2}Tr\{X + r_xX^2 + r_yXY + r_zXZ\} && (3.38)\\
&= \frac{1}{2}r_xTr\{I\} && (3.39)\\
&= r_x. && (3.40)
\end{aligned}$$

We can see that the expectation value can be written as the trace of the operator times the state. So, to perform a state tomography of a single qubit, we first need to prepare thousands of copies of the unknown state ρ. Then measure some portion of the states in Pauli X basis, Z basis, and Y basis to obtain the estimates of the Bloch vector components which is given by $(\bar{r_x}, \bar{r_y}, \bar{r_z})$. After that we have to re normalize the vector since the Bloch vector components obtained, are estimates and not the actual values. That can be done by diving the estimates by the length of the vector as

$$(\bar{r_x}, \bar{r_y}, \bar{r_z})/\sqrt{\bar{r_x}^2 + \bar{r_y}^2 + \bar{r_z}^2}. \tag{3.41}$$

For two-qubit state, we can write the output state as

$$\rho = \frac{1}{4}\sum_{j,k=0}^{3} \langle \sigma_j \otimes \sigma_k \rangle \sigma_j \otimes \sigma_k. \tag{3.42}$$

where $(\sigma_0, \sigma_1, \sigma_2, \sigma_3) = (I, X, Y, Z)$. Therefore, 15 measurement setting are required, since we are considering 4 basis. On the actual device, we do not need to measure the I operator. So, precisely we only measure them in 9 measurement basis for two-qubit system. For N qubits, $4^N - 1$ measurement settings are needed. To know the full knowledge of the states, we need to perform multiple measurements for all of these exponential measurement settings. Therefore, performing state tomography is a very resourceful process and computationally expensive [46]. It is only suitable for small systems. Beside the substantial amount of the resource required, in order to perform tomography, we have to measure the link itself. This consumes the link and prevent us from using the application. To tackle this two problem, Maity et al have come up with a unique way which uses different protocol with different intention at site.

3.4 Proposed Approach: Maity et al's Protocol

Maity et al came up with a new approach [33] to solve the problem of the heavy resource cost and stoppage of application, using the purification protocol [3]. The purification protocol's original usage in quantum network communication was to improve the fidelity of the entangled link. Over the course of the protocol's procedure, there are classical results that are thrown away. Maity et al's protocol uses this result, was thought to be a garbage, with the equation they derived which makes the estimation of Pauli errors possible in entangled link. This section explains the purification protocol, how Maity et al's protocol estimates the error probability, and the certain assumption we made in this project, using the success rate of the purification protocol.

3.4.1 Purification Protocol

Purification or quantum purification detects the Pauli errors and improves the quality, fidelity in particular, of the entangled link. The purification protocol was first proposed by Bennett et al in 1996 [3]. Protocol schemes with more advanced operations have been proposed as well [17]. Entanglement purification has been demonstrated on different physical devices; superconducting devices [47] [49], and linear optical devices [38]. The significance of the procedure lies in its applicability without destroying the entangled state.

X purification is the X-error purification which is a particular purification scheme to detect Pauli X and Y errors. Some people refer to them as the Z-basis purification since we do the measurement operation in the Pauli Z basis. However, to avoid confusion, in this paper, we refer to them as the X purification.

Figure3.2 illustrates the procedure of the basic X purification. First we share two copies of the entangled state between two party (qubit), often referred to as Alice and Bob. In the figure 3.2, qubits A_0 and B_0 are entangled and qubits A_1 and B_1 are entangled. Then Alice and Bob applies a local operations on their bipartite entangled qubits; CNOT operation and Pauli Z basis measurement on the same bipartite entangled pair. Then, they exchange the classical result information they measured. This allows for them to find out information about the entangled Bell pair that is not measured and even further improves the fidelity of it. When Alice and Bob both share entangled states without error, the protocol can be represented mathematically as

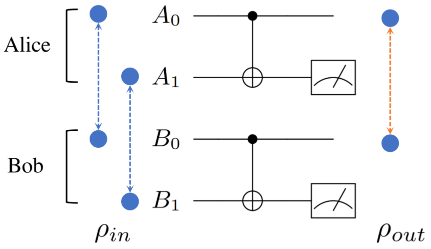

Figure 3.2: X purification protocol [2]

$$|\Phi^+\rangle_{A_0B_0}|\Phi^+\rangle_{A_1B_1} = (|00\rangle + |11\rangle)(|00\rangle + |11\rangle) \tag{3.43}$$
$$= |00\rangle|00\rangle + |00\rangle|11\rangle + |11\rangle|00\rangle + |11\rangle|11\rangle \tag{3.44}$$
$$CNOT_A \rightarrow |00\rangle|00\rangle + |00\rangle|11\rangle + +|11\rangle|10\rangle + |11\rangle|01\rangle \tag{3.45}$$
$$CNOT_B \rightarrow |00\rangle|00\rangle + |00\rangle|11\rangle + +|11\rangle|00\rangle + |11\rangle|11\rangle \tag{3.46}$$
$$= |\Phi^+\rangle_{A_0B_0}|\Phi^+\rangle_{A_1B_1}. \tag{3.47}$$

$|\Phi^+\rangle_{A_0B_0}$ is the first Bell pair shared between Alice and Bob and $|\Phi^+\rangle_{A_1B_1}$ is the second Bell pair shared between the two. After measuring the second pair in the Pauli Z basis, it will give us the classical result of 00 with the probability of 1/2 and 11 with the probability of 1/2. We can see that the outcomes are correlated so they will keep the first pair. When the first Bell pair is affected by the bit flip error, the protocol can be written mathematically as

$$|\Psi^+\rangle_{A_0B_0}|\Phi^+\rangle_{A_1B_1} = (|01\rangle + |10\rangle)(|00\rangle + |11\rangle) \tag{3.48}$$
$$= |01\rangle|00\rangle + |01\rangle|11\rangle + |10\rangle|00\rangle + |10\rangle|11\rangle \tag{3.49}$$
$$CNOT_A \rightarrow |01\rangle|00\rangle + |01\rangle|11\rangle + +|10\rangle|10\rangle + |10\rangle|01\rangle \tag{3.50}$$
$$CNOT_B \rightarrow |01\rangle|01\rangle + |01\rangle|10\rangle + +|10\rangle|10\rangle + |10\rangle|01\rangle \tag{3.51}$$
$$= |\Psi^+\rangle_{A_0B_0}|\Psi^+\rangle_{A_1B_1}. \tag{3.52}$$

As seen from the equation, the error of the first pair got propagated to the second pair that we will measure. When we measure the second pair, we will get the classical result of 01 or 10, with probability of 1/2.

Summarizing the procedure, by conducting the operations and exchanging the classical information, they check if the protocol was successful and decides to keep or discard the first entangled pair. If they both measure the same result, 00 or 11, it is correlated, so they will keep the result. If they measure different result, 01 or 10, they can discard the state. Table 3.1 shows the results and actions of the protocol for each scenario. When both pairs do not have the error, that occurs with the probability of F^2 from equation 3.30. The probability of only one pair having the noise is $(1-F)F$ or $F(1-F)$. The probability of both pair having the noise is $(1-F)^2$. We have to note that even when both state is affected by the noise, it will give us the correlated classical result.

Pair 1	Pair 2	Probability	Measurement result	Action	Result
$\|\Phi^+\rangle$	$\|\Phi^+\rangle$	F^2	00 or 11	Keep	$\|\Psi^+\rangle$
$\|\Phi^+\rangle$	$\|\Psi^+\rangle$	$F(1-F)$	01 or 10	Discard	N/A
$\|\Psi^+\rangle$	$\|\Phi^+\rangle$	$(1-F)F$	01 or 10	Discard	N/A
$\|\Psi^+\rangle$	$\|\Psi^+\rangle$	$(1-F)^2$	00 or 11	Keep	$\|\Psi^+\rangle$

Table 3.1: X purification results

Which means, the probability of successful procedure is given by $F^2 + (1-F)^2$. Therefore the output fidelity F' when the initial fidelity is F, is given by

$$F' = \frac{F^2}{F^2 + (1-F)^2}. \tag{3.53}$$

From the equation, the F' will only be greater than the initial fidelity F, only when $F > 0.5$. We can do this procedure multiple times and increase the fidelity as much as possible. The successfully purified state that Alice and Bob keeps, could be expressed as

$$\rho' = F' |\Phi^+\rangle \langle\Phi^+| + (1-F') |\Psi^+\rangle \langle\Psi^+|. \tag{3.54}$$

using the improved fidelity F'.

Similary, Z purification will detect phase flip error (Z error) and Y error. Y purification will detect X and Z error. Each purification circuit are shown in figure 3.3, 3.4, 3.5.

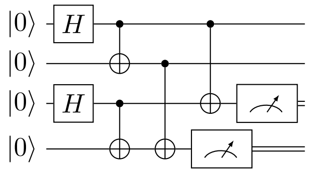

Figure 3.3: X purification circuit

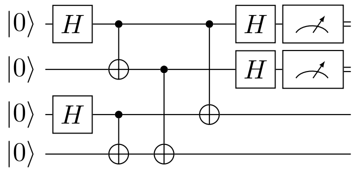

Figure 3.4: Z purification circuit

In practice, we take the distribution of the states. Maity et al's protocol uses the success rate of the purification, s_x, for classical result of 00. For example, we do the same X purification 10000 times and get the classical result of {00} 4000 times, {11} 4000 times, {01} 1000 times, and {11} 1000 times. The success rate s_x will be (3000)/10000 = 0.3. Success rate in Z and Y purification basis could be denoted as s_z and s_y.

3.4.2 Werner State

In the real world device, the three different Pauli errors could have different probabilities and could be written as

$$\rho = p_1 |\Phi^+\rangle \langle\Phi^+| + p_x |\Psi^+\rangle \langle\Psi^+| + p_z |\Phi^-\rangle \langle\Phi^-| + p_y |\Psi^-\rangle \langle\Psi^-|. \tag{3.55}$$

Notice that Y error is the combination of X and Z errors. However, in this project, to start with a simple problem, I estimated the Pauli errors under the assumption that they are equal as $p_w = p_x = p_z = p_y$. p_w is the Werner error probability and such assumption is called the Werner assumption. This means in equation 3.55, $p_1 + p_x + p_z + p_y = 1$. Such state could be written using the fidelity as

$$\rho_w = F |\Phi^+\rangle \langle\Phi^+| + (\frac{1-F}{3}) |\Psi^+\rangle \langle\Psi^+| + (\frac{1-F}{3}) |\Phi^-\rangle \langle\Phi^-| + (\frac{1-F}{3}) |\Psi^-\rangle \langle\Psi^-| \tag{3.56}$$

$$= F |\Phi^+\rangle \langle\Phi^+| + \frac{1-F}{3}(|\Psi^+\rangle \langle\Psi^+| + |\Phi^-\rangle \langle\Phi^-| + |\Psi^-\rangle \langle\Psi^-|), \tag{3.57}$$

$$= (1-3p_w) |\Phi^+\rangle \langle\Phi^+| + p_w(|\Psi^+\rangle \langle\Psi^+| + |\Phi^-\rangle \langle\Phi^-| + |\Psi^-\rangle \langle\Psi^-|). \tag{3.58}$$

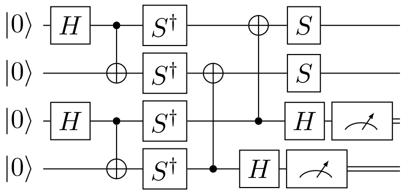

Figure 3.5: Y purification circuit

The fidelity of the Werner state would be $F = 1 - 3p_w$. For estimating the Werner error parameter, only one of the Pauli purification scheme is needed.

However, to estimate all different Pauli error parameters one purification scheme is not enough. For example, in the Bell diagonal state from equation 3.55, there are three unknown parameters. To verify all of them all three purification schemes are needed.

3.4.3 Estimation of the Werner error parameter

Maity et al derived an equation which showed the relation between the success rate of the purification s and the Werner error probability as

$$s = \frac{1}{2}(1 - 4p_w + 8p_w^2) \tag{3.59}$$

By obtaining the statistic success rate by running either purification scheme, we can get s_x, s_z, s_y. Then, the Werener parameter can be obtained by substituting it into

$$p_w = \frac{1 - \sqrt{4s - 1}}{4} \tag{3.60}$$

where p_w is the Werner parameter. This is my approach to solve the first problem of this project which is estimating the Werner error parameter in the entangled link, using the purification protocol.

3.5 Testing on Actual Device

So far, I have explained about my first problem and how I will solve it. In this section it aims to clarify the second problem, which is actually implementing the idea of the first problem on actual quantum device. When we consider simulation of entangled link and protocol to be implemented on actual quantum device, there are several candidates of quantum devices to be tested. They are devices that can process these information physically such as the superconducting qubits (Cooper-pair box [36], Transmon [28] [23]), trapped ions [16] [6], and linear optical qubits [27]. Any quantum system that satisfy the DiVincenzo criteria introduced in 2000 [12] could be a quantum computer. DiVincenzo criteria says that if you want to build a normal quantum computers you need to have the following things.

1. Well-defined scalable qubit.
2. Qubits can be initialized.
3. Long relevant lifetime of qubits, longer than gate operation time.
4. Universal quantum gate set.
5. Efficient measurement of qubits.

For quantum communication, addition to above, we also want to convert or entangled stationary and flying qubits, and able to carry flying qubits long distances. For the such stationary qubit, the Nitrogen-vacancy center in diamond [7, 25]is one of the candidate for memory qubit and is what AQUA is aiming to use (maybe add silicons). There is also an approach to communicate between superconducting qubits through photonic conversions [30]. These are all candidates that are worth testing Maity et al's protocol.

Out of all the candidates, in this project I will test the Maity et al's protocol on IBM quantum device which is accessible by cloud computing. IBM quantum computers are accessible to many but not all researchers and students around the world [9] [24].

Chapter 4

Methodology and Evaluation

In this chapter, I will explain the specific methods and procedures to solve the two problems introduced in the previous chapter. Simply speaking, that is, how I actually estimated the Werner error parameter on actual device. In theory, it was simply explained, but in order to test it on actual device, I needed to evaluate the codes made on the simulator first. Then, also showed how I verified the estimate obtained from the actual device.

4.1 setup

I used the IBM Qiskit library [42], an library to control the IBM quantum computers through cloud, using the programming language, Python. I tested the codes that I translated from the protocol on the simulators first and then on the actual IBM device. Additionally, to check if the simulator codes were reliable, I tested the traditional approach, performing state tomography, to evaluate it. For the simulator, I used the AerSimulator. For the actual quantum device, I used IBM Q Kawasaki.

4.2 Running Purification and Estimating Werner Error

In this section, I will explain how I ran purification and estimated the Werner error probability. To test the code on actual device, I first needed to make the code for the simulator. First, I had to make the code for doing the reverse of the estimate, which was make the code that actually controlled the error parameters and see the success rate and the fidelity of the simulated entangled link. This is in purpose to check if the purification code worked properly. To set a Werner state error model, I first needed to be able to set the error probability of three Pauli errors to be equal. So I implemented the individual Pauli error model on the simulator first. I also made codes for each Pauli purification schemes. For estimating the Werner parameter, one purification scheme is sufficient, but each purification scheme gave me different success rate, so I compared them as well. Plus, eventually, all three purification scheme will be required to estimate each error probability for the Bell diagonal state (equation 3.55).

4.2.1 Purification Circuit and Pauli Error Models on Simulator

First, I coded the circuit for X purification on figure 4.1 and ran it on the AerSimulator. Using the Qiskit Aer Noise Module, I inserted an error model gate (I gate on figure 4.1) to the circuit which controlled the probability of the bit flip error. I ran the X purification simulator code, setting the bit flip error parameter to vary between 0 and 1, in 0.05 step size. I ran the circuit with 10000 shots. This will give us the result of the classical bits measured for the second Bell pair and the improved fidelity after the purification. I expected the correlated classical results 00 and 11 for low error probability and the anti correlated results, 01 and 10, for the high error probability trials. I also expected the fidelity to improve when the error probability was below 0.5.

Then, I made the simulator circuit for Z purification and Y purification on figures 4.2, 4.3. After that, I introduced phase flip noise and bit phase flip noise for each purification circuit. As I did for the X purification circuit and bit flip error model, I ran it with each error parameter varying between 0 and 1, in 0.05 step size. I also ran the circuits with 10000 shots. For the Y purification circuit with bit phase flip error model, I did not expect correlated classical result, since

Y purification, regardless of its name, does not detect the bit flip (Y) error, but instead detects X and Z errors.

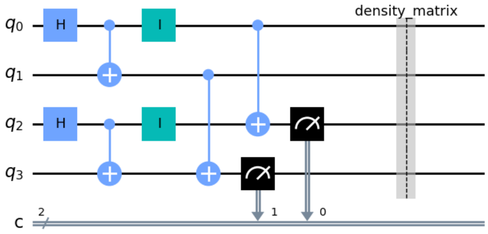

Figure 4.1: Implemented X purification circuit

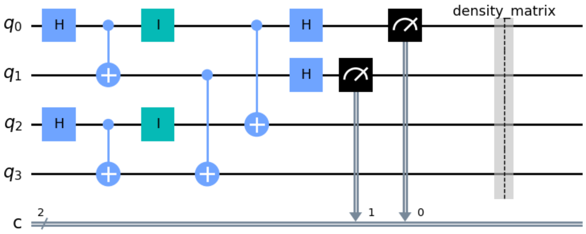

Figure 4.2: Implemented Z purification circuit

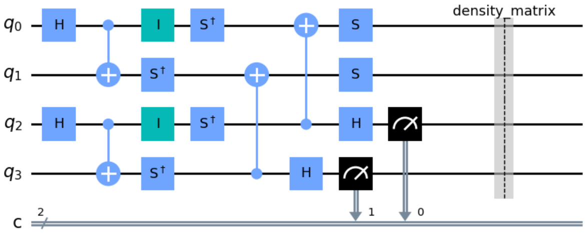

Figure 4.3: Implemented Y purification circuit

Evaluation

To check if each of the error models were successfully implemented, I performed a state tomography on the unmeasured Bell pair, using the Qiskit Experiment [41], a module provided by IBM Qiskit. By performing the state tomography, I can construct the density matrix of the Bell pair and see if the errors were successfully implemented or not. If a bit flip is successfully implemented, when running the circuit multiple times, the original Bell state $|\Phi^+\rangle$ will be flipped and have $|\Psi^+\rangle$ depending on the parameterized error probability, p. Each density matrix after performing state tomography on Pauli error channels can be computed theoretically as follows; density matrix of entangled link without any error or all Pauli error probability being 0 is

$$|\Phi^+\rangle\langle\Phi^+| = \frac{1}{2}\begin{bmatrix} 1 & 0 & 0 & 1 \\ 0 & 0 & 0 & 0 \\ 0 & 0 & 0 & 0 \\ 1 & 0 & 0 & 1 \end{bmatrix}, \tag{4.1}$$

with bit flip error p is

$$(1-p)\left|\Phi^+\right\rangle\left\langle\Phi^+\right| + p\left|\Psi^+\right\rangle\left\langle\Psi^+\right| = \frac{1}{2}\left\{\begin{bmatrix}1-p & 0 & 0 & 1-p\\ 0 & 0 & 0 & 0\\ 0 & 0 & 0 & 0\\ 1-p & 0 & 0 & 1-p\end{bmatrix} + \begin{bmatrix}0 & 0 & 0 & 0\\ 0 & p & p & 0\\ 0 & p & p & 0\\ 0 & 0 & 0 & 0\end{bmatrix}\right\} \tag{4.2}$$

$$= \frac{1}{2}\begin{bmatrix}1-p & 0 & 0 & 1-p\\ 0 & p & p & 0\\ 0 & p & p & 0\\ 1-p & 0 & 0 & 1-p\end{bmatrix}, \tag{4.3}$$

with phase flip error p is

$$(1-p)\left|\Phi^+\right\rangle\left\langle\Phi^+\right| + p\left|\Phi^-\right\rangle\left\langle\Phi^-\right| = \frac{1}{2}\left\{\begin{bmatrix}1-p & 0 & 0 & 1-p\\ 0 & 0 & 0 & 0\\ 0 & 0 & 0 & 0\\ 1-p & 0 & 0 & 1-p\end{bmatrix} + \begin{bmatrix}p & 0 & 0 & -p\\ 0 & 0 & 0 & 0\\ 0 & 0 & 0 & 0\\ -p & 0 & 0 & p\end{bmatrix}\right\} \tag{4.4}$$

$$= \frac{1}{2}\begin{bmatrix}1 & 0 & 0 & 1-2p\\ 0 & 0 & 0 & 0\\ 0 & 0 & 0 & 0\\ 1-2p & 0 & 0 & 1\end{bmatrix}, \tag{4.5}$$

with bit phase flip error p is

$$(1-p)\left|\Phi^+\right\rangle\left\langle\Phi^+\right| + p\left|\Psi^-\right\rangle\left\langle\Psi^-\right| = \frac{1}{2}\left\{\begin{bmatrix}1-p & 0 & 0 & 1-p\\ 0 & 0 & 0 & 0\\ 0 & 0 & 0 & 0\\ 1-p & 0 & 0 & 1-p\end{bmatrix} + \begin{bmatrix}0 & 0 & 0 & 0\\ 0 & p & -p & 0\\ 0 & -p & p & 0\\ 0 & 0 & 0 & 0\end{bmatrix}\right\} \tag{4.6}$$

$$= \frac{1}{2}\begin{bmatrix}1-p & 0 & 0 & 1-p\\ 0 & p & -p & 0\\ 0 & -p & p & 0\\ 1-p & 0 & 0 & 1-p\end{bmatrix}. \tag{4.7}$$

I expect to see the corresponding density matrix for each Pauli error models ran.

4.2.2 Werner Error Model on simulator

To make the Werner error model I needed to have each Pauli error probability to be equal. So, I set the error noise gate (I gate) on each purification scheme from figures 4.1, 4.2, 4.3 to $(1-3p)$, where p = bit flip error probability = phase flip error probability = bit phase flip error probability. I ran each purification scheme, setting the parameter to vary between 0 and 1, in 0.05 step size. For the classical result, I expect something similar to the first scenario where I just introduced the Pauli errors individually. However, for the Y purification circuit it should also show successful corresponding results as bit flip and phase flip error was introduced in the Werner error model. The fidelity should also improve as well when the error probability is low.

Evaluation

In order to check if the Werner error model was successfully implemented, I performed state tomography on the unmeasured Bell Pair and examined if the ideal density matrix was constructed. The ideal density matrix of a Bell Pair when the Werner error model is successfully implemented is

$$(1-3p)\left|\Phi^+\right\rangle\left\langle\Phi^+\right| + p(\left|\Psi^+\right\rangle\left\langle\Psi^+\right| + \left|\Phi^-\right\rangle\left\langle\Phi^-\right| + \left|\Psi^-\right\rangle\left\langle\Psi^-\right|) \tag{4.8}$$

$$= \frac{1}{2}\left\{\begin{bmatrix}1-3p & 0 & 0 & 1-3p\\ 0 & 0 & 0 & 0\\ 0 & 0 & 0 & 0\\ 1-3p & 0 & 0 & 1-3p\end{bmatrix} + \begin{bmatrix}0 & 0 & 0 & 0\\ 0 & p & p & 0\\ 0 & p & p & 0\\ 0 & 0 & 0 & 0\end{bmatrix} + \begin{bmatrix}p & 0 & 0 & -p\\ 0 & 0 & 0 & 0\\ 0 & 0 & 0 & 0\\ -p & 0 & 0 & p\end{bmatrix} + \begin{bmatrix}0 & 0 & 0 & 0\\ 0 & p & -p & 0\\ 0 & -p & p & 0\\ 0 & 0 & 0 & 0\end{bmatrix}\right\} \tag{4.9}$$

$$= \frac{1}{2}\begin{bmatrix}1-2p & 0 & 0 & 1-4p\\ 0 & 2p & 0 & 0\\ 0 & 0 & 2p & 0\\ 1-4p & 0 & 0 & 1-2p\end{bmatrix}, \tag{4.10}$$

when p is the error parameters of each Pauli errors (Werner error probability). I expect the density matrix to be similar, when running the Werner state error model on each purification circuit.

4.2.3 Purification on Actual Device

After checking the codes ran without an issue for the simulator, I implemented each purification scheme on actual device. Assuming that the channel was a Werner state and using the classical count results, I estimated the error probability. I substituted each success rate obtained after running three purification scheme to the Maity at el's equation 3.60. I expect to see lower error probability estimate for X purification, compared to Z and Y, since it uses less gates which could potentially introduce less coherent errors in real device.

4.3 Verification of the Estimate

This section explains how I evaluated the estimated Werner probability. In order to check how well the estimation was done, we computed the fidelity between the Werner assumed purified circuit and a simple entangled Bell Pair. This is because the simple entangled Bell pair will resemble the actual entangled link and the purified circuit to resemble the Werner assumption that had the purification in practice. I performed state tomography on both circuit to construct the density matrix needed to derive the fidelity.

4.3.1 Simulation of Entangled Link

After making a simple $|\Phi^+\rangle$ (Figure 3.1) code on a simulator, I ran it on IBM Kawsaki with 10000 shots, and performed state tomography. This is for checking if the simulation of an actual entangled link was properly created. The density matrix should look something similar to equation 4.3. Take into note, that this is the traditional way of actually characterizing the errors as mentioned in chapter 3. You can see that there is no more link to be used, for the application, as it did not propagate and keep the state as we do in the purification protocol. After checking the implementation of a simple entangled link, I ran the code to verify the estimate, which will be explained in the next section.

4.3.2 Fidelity of Bell Pair and Purified Bell Pair on Actual Device

To check how close the estimation was to the actual link, I performed state tomography on a non-purified Bell Pair and a purified Bell pair and computed the fidelity between them on IBM Kawasaki. The non-purified Bell Pair represent the actual link channel that will be used for network. If the fidelity is close to 1, that means the estimation made over Werner assumption was relatively accurate on IBM device. I did this for all three purification schemes. I do not expect a fidelity totally identical to 1 since on the actual entangled state, the Pauli errors are most likely not equal. I expect the estimate to be more accurate for the X purification, compared to Z and Y purification as it used less gates.

Chapter 5

Result and Discussion

This chapter will share and discuss the results of the setups introduced in chapter 4.

5.1 Estimated Result of Werner Error

5.1.1 Individual Pauli Error Model and Purification Result on Simulator

Figure 5.1 is the measurement output of X purification with bit flip error model, when $p = 0.1$. p being the bit flip error probability, I ran it on the AerSimulator. As shown in the figure, in the case of $p = 0.1$, we got 4136 counts of $\{00\}$ and 4066 counts of $\{11\}$. This means, the protocol was successful $4136 + 4066 = 8202$ times out of 10000. Furthermore, we got 899 counts of $\{01\}$ and 899 counts of $\{10\}$. This means, for $899 + 899 = 1798$times, it had either the phase flip (Z) error or bit phase flip (Y) error. This is as expected, since the error probability is $p = 0.1$, the fidelity F is 0.9. From Table 3.1, the probability of protocol successfully passing is $F^2 + (1 - F)^2$, therefore we will get approximately $0.81 + 0.01 = 0.82$ probability of $\{00\}$ and $\{11\}$ counts. Figures 5.2 shows the measurement output Z and Y purification with phase flip and bit phase flip error model, when $p = 0.1$. p being the phase flip and bit phase flip error probability. For the Z purification result, similarly to the X purification, the purification scheme detected either the bit flip (X) error or bit phase flip (Y) error, $934 + 900 = 1834$ times. For the Y purification result, as expected, it only gave us a correlated result because Y purification only detects X and Z error and not the Y error which was implemented as the error model.

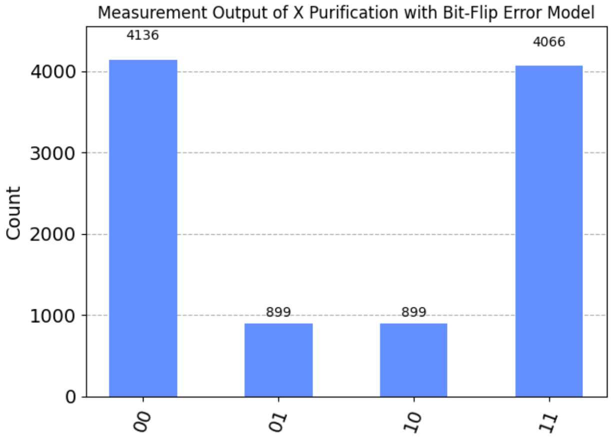

Figure 5.1: Classical result of X Error Model on Simulator

Figure 5.3 shows the initial and improved fidelity, when the bit flip error probability was set from 0 to 1, in 0.05 step size. As you can see from the figure, the improved fidelity F' only gives us a higher fidelity, when the initial fidelity F is larger than 0.5 as theory explained from equation 3.53.

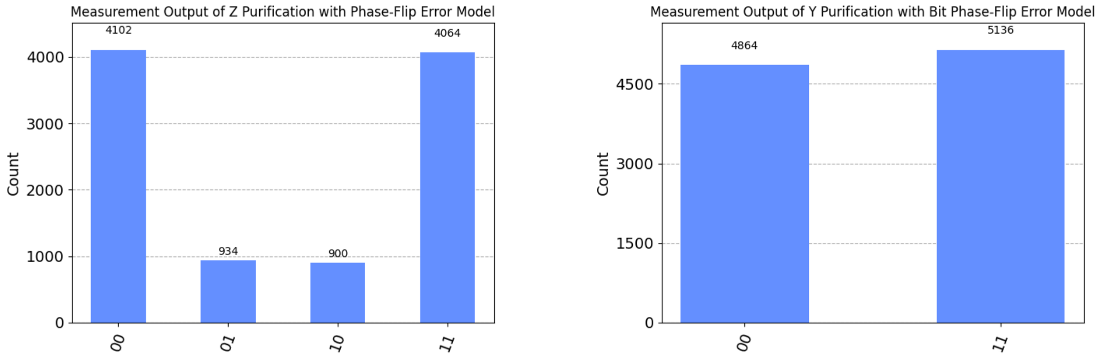

(a) Z

(b) Y

Figure 5.2: Shot Results of Each Error Model on Simulator

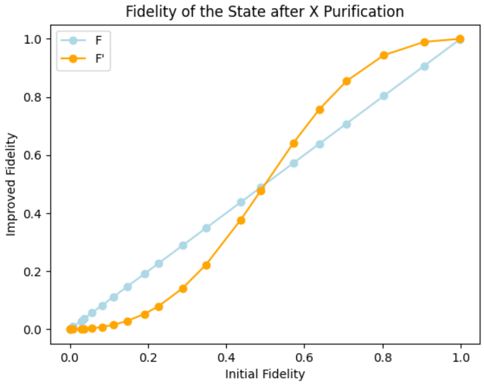

Figure 5.3: Fidelity Result for Each Purification Scheme X

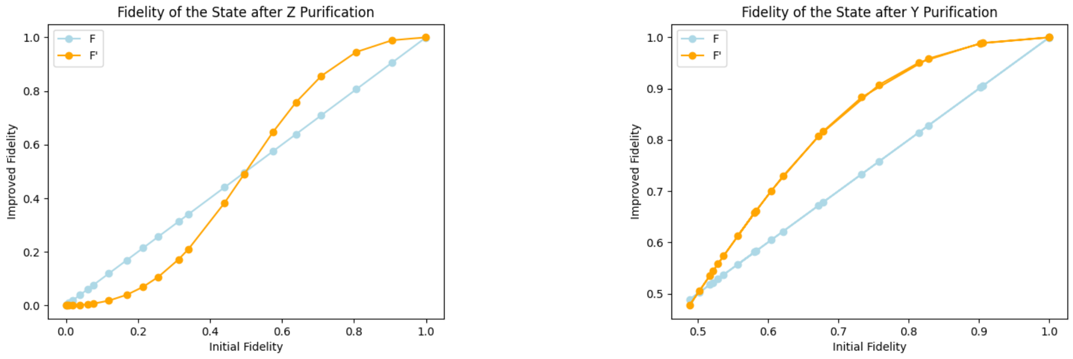

(a) Fidelity with phase flip error model

(b) Fidelity with bit phase flip error model

Figure 5.4: Fidelity Result for phase and bit phase error on simulator

Similar results were seen for the Z purification with Z error as shown in figure 5.4a. For the Y purification in figure 5.4b, when setting the bit phase flip error probability to either high or low, the initial fidelity will be higher than 0.5 as Y purification only detects X and Y errors. Therefore, the improved fidelity was always higher than the initial fidelity.

From these classical results and fidelity results, I was able to see the purification schemes implemented successfully.

Evaluation

Now that I was able to see the purification schemes successfully being implemented, I performed state tomography on the unmeasured Bell pair of the purified circuit for each error model, to check if the error model was successfully implemented. Figure 5.5 is the visualization of the state tomography result for bit flip error model on X purification circuit, when bit flip error probability is 0.1. The density matrix matches the theoretical density matrix, from equation 4.3, when bit flip error probability $p = 0.1$. Similarly, Figure 5.6a and Figure 5.6b shows the result for phase flip error model on Z purification circuit and bit phase flip error model, when $p = 0.1$. The density matrix matches the theoretical density matrix, from equation 4.5 and (4.7), when each error probability is 0.1. From these results, I was able to confirm that each Pauli error model was successfully implemented on the simulator.

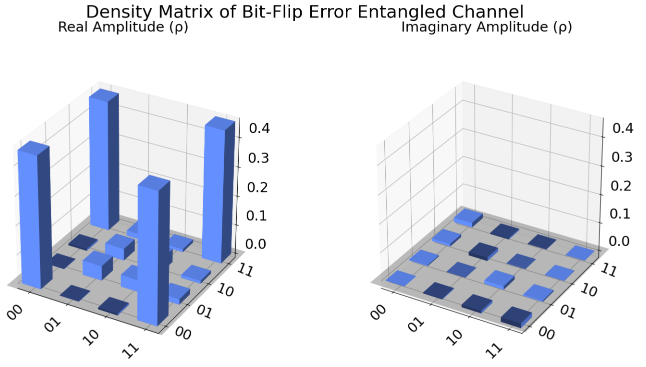

Figure 5.5: State Tomography Result for Bit flip Error Model

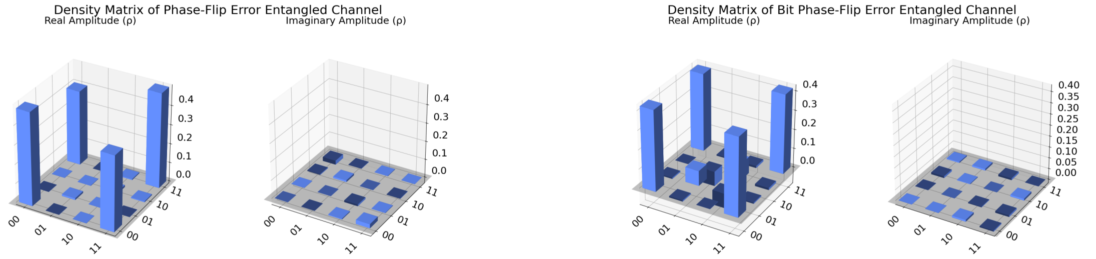

(a) State Tomography Result for Phase flip Error Model

(b) State Tomography Result for Bit phase flip Error Model

Figure 5.6: State tomography result on simulator

5.1.2 Werner Error Model Result on simulator

After seeing the successful implementation of each Pauli error models, using that code, I made the code for Werner error model, as explained, and ran the error model on each purification scheme on a simulator. Figure 5.7 shows the classical shot result of the Werner error model ran with X purification circuit, when $p = 0.1$. As expected, since the error probability for bit, phase, bit phase flip error was introduced, the protocol was successful. Same thing was visible in Z and Y purification scheme. Notice that Y purification also showed similar result because unlike the bit phase flip error, the Werner error model had all three Pauli errors equally. From this result, I was able to see that each purification scheme also worked properly for Werner error model.

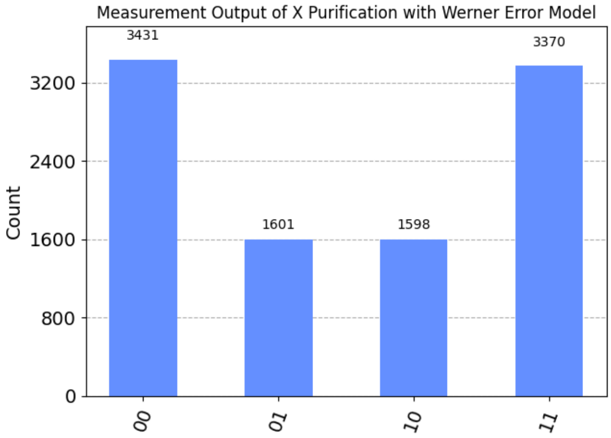

Figure 5.7: Shot Result of Werner Error Model on Simulator

Evaluation

Now that I was able to see the proper function of each purification scheme on the Werner error model, I checked if the Werner error model was working properly. Figure 5.8 shows the density matrix of Werner entangled channel when $p = 0.7$. This matches the theoretical density matrix of euation (4.10). Therefore, I was able to be sure that the Werner error model was functioning properly.

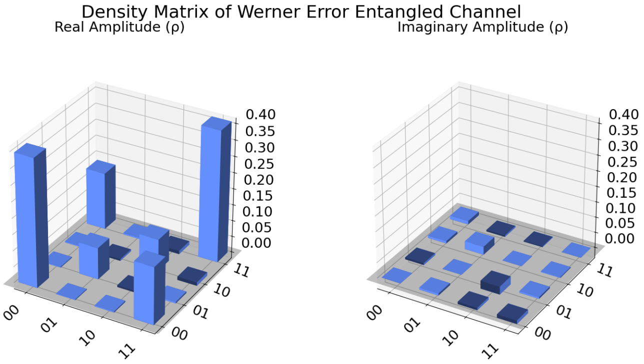

Figure 5.8: State Tomography Result of Werner Error Model X Purification on Simulator

5.1.3 Purification Result on IBM Kawasaki

Now that I was able to confirm that purification code functioned properly on Werner error model, I ran it on the actual quantum device, IBM Kawasaki. Figure 5.9 shows the measurement outcome of X purification with 10000 shots. From the figure we can see that the protocol was successful for $4769 + 4621 = 9390$ times. The success rate $s_x = 4769/10000 = 0.4769$. Substituting this into equation 3.60 we can obtain the Werner error probability which was $w_X = 0.011829892723708935$. Werner error probability estimate using Z purification and Y purification could be computed

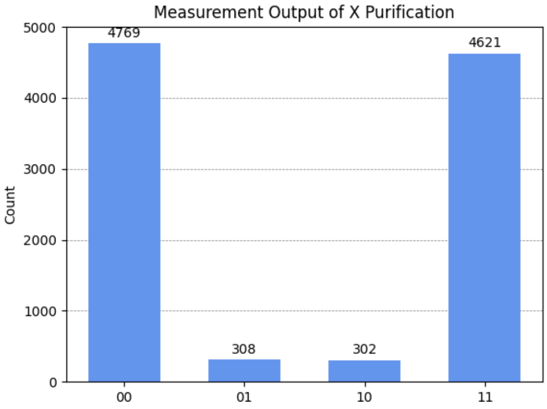

Figure 5.9: Shot Result of X purification on IBM Kawasaki

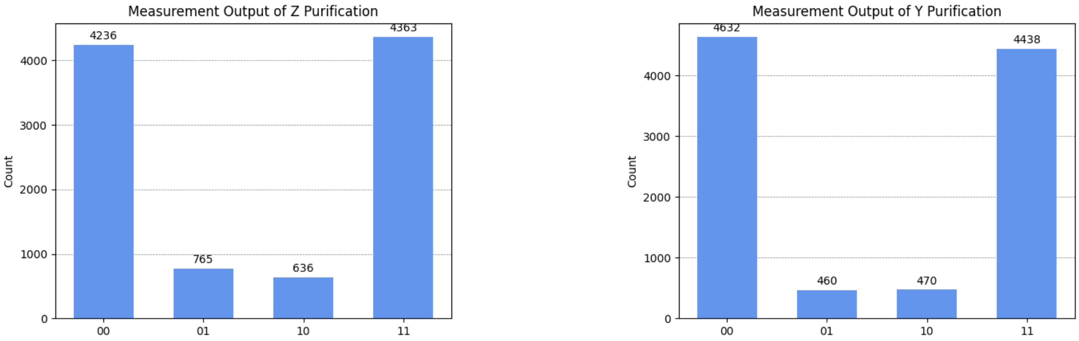

(a) Z purification

(b) Y purification

Figure 5.10: Shot results on IBM Kawasaki

similary, using the result from Figures 5.10a and 5.10b. Each Werner probability estimate was $w_Z = 0.041673333440003\,43$ and $w_Y = 0.019132072387696097$.

As expected, w_X was lower than x_Z and x_Y, probably due to the number of gates used in the purification. w_X uses more gates in the circuit to do the purification which could have introduced more noise to the channel. To truly analyze the reason, I will need to examine the universal gates and other noises such as depolarizing noises and thermal noises. Similary, w_Y was higher than w_X, as it uses less gates in the IBM's actual physical system.

5.2 Verification of the Estimate

Now, to verify the estimated value, I obtained the fidelity between a simple simulated entangled state ran on IBM Kawasaki and purified Bell Pair on actual device with each scheme.

5.2.1 Simple Bell Pair State Tomography on IBM Kawasaki

The density matrix result of a simple pre-purified entangled state constructed by performing state tomography is on Figure 5.11. As it matches the expected noisy result, similar to equation 4.7, I was able to confirm that entangled link was ideally simulated.

5.2.2 Fidelity of Bell Pair and Purified Bell Pair on IBM Kawasaki

After confirming that the entangled link was ideally simulated, I obtained the fidelity between each purification scheme. This tells us about the validity of the estimate using each scheme and results are shown on figre 5.12. Interestingly, the result shows that that the Y purification scheme had a better Werner estimate than the Z purification scheme. It also shows that the X purification scheme was the best as well.

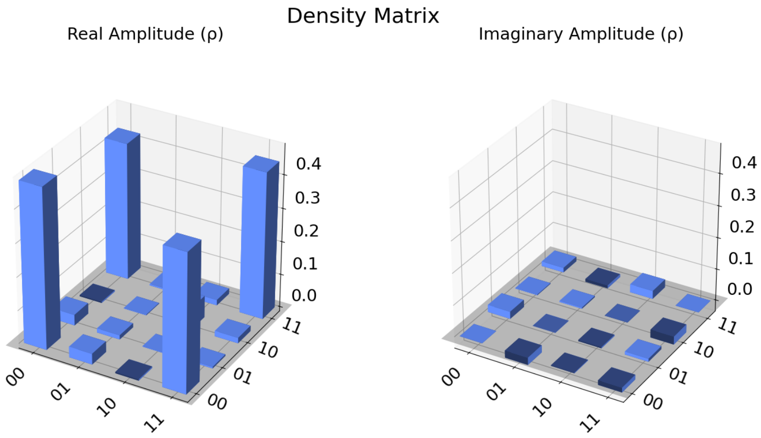

Figure 5.11: State tomography result of simulated pre-purified entangled link

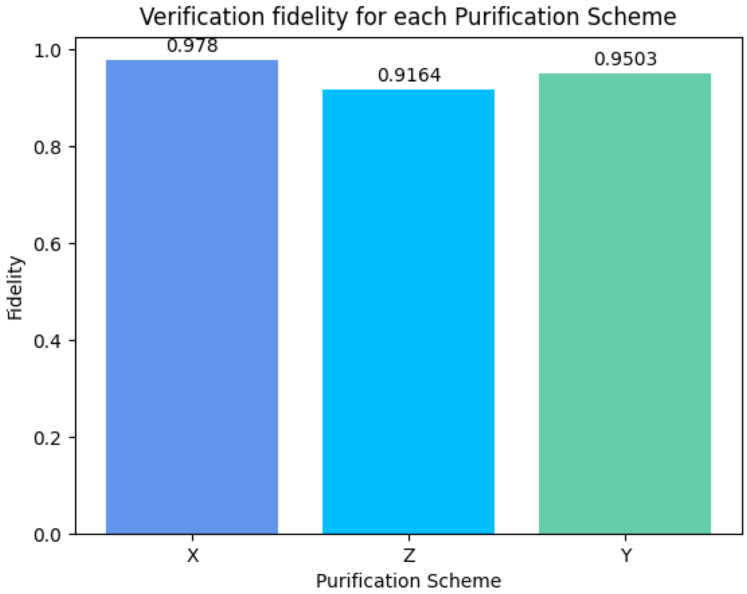

Figure 5.12: Verification result on IBM Kawasaki

Chapter 6

Conclusion and Remarks

6.1 Analysis Summary

As mentioned in section 5.1.3, I was able to estimate the Werner error probability using the equation by Maity et al and the measurement result obtained from the purification protocol. This signifies that I was able to characterize the Pauli errors on actual quantum device. However, we have to take into note that this was done only under the Werner assumption. To characterize individual Pauli error probability, I will need to do further calculation. It will require all three purification scheme (X purification, Z purification, and Y purification). I did have the measurement result for them, but I did not make the simulation circuit for the Bell diagonal state, therefore, did not include it in this thesis but could be a possible future work. With that, my first problem of tackling the efficient method to characterize the Pauli errors within the entangled simulated link was accomplished.

My second criteria of testing them on actual device was satisfied as well, as I was able to obtain the Werner parameter as the theory suggested. From Figure 5.12, it did not only estimate the Werner parameter, but also showed us that X purification will be the best circuit to just estimate the Werner error probability.

6.2 Future Work

As mentioned one future work will be to test the protocol to estimate individual Pauli errors. However, since we were able to know that the Maity at el's protocol actually works on real quantum device, this signifies that the Maity at el's protocol can be used to test the performance of quantum devices as well. This time, I only tested with single IBM quantum device, IBM Kawasaki, but it could be tested on other IBM quantum device as well. Not only limiting it to superconducting physical qubits, the method could potentially be used to other physical system, such as the ion trap quantum computers. By simulating the entangled link for quantum network, it could possibly set the bench mark for suitable physical system and types of nodes or repeaters in the quantum network.

Furthermore, I could do the protocol even more with just the Werner assumption as well. On the circuit, the purification protocol looks simple by just applying the CNOT gate over two bi-partied entangled qubits, however on the actual physical layout of IBM, in order to perform CNOT between the non-neighboring qubits, entanglement swapping is done which introduces us to a connectivity problem. To get around that problem, we can use the measurement based quantum computing (MBQC) [22] in graph state to chain the non-neighboring qubits to create an entanglement. This long chained entanglement could also presumable have lower quality of entanglement, therefore could simulate a scenario closer to the actual quantum network, where we purify different quality entangled links.

Acknowledgment

I want to thank everyone who got involved with me till today. I want to thank my boss, Professor Rodney Van Meter for making AQUA and letting me have the opportunity to interact with the world's most interesting people. I deeply want to thank two of my mentor, Hajdusek Michal and Naphan Benchasattabuse(whit3z) for being the ideal mentors. Michal, I thank you for guiding me in right direction and being patient with my immature and ignorant questions. Whit3z, I thank you for giving me important insights and helping me when I was stuck. It was fun discussing things beyond the project with you as well.

I want to thank, Poramet Pathumsoot and Makoto Nakai(Dave) for helping me with code implementation when I was stuck too. I also want to thank other AQUAnauts and all friends from SFC campus, making my Graduation Project a ”fun” thing, instead of a completely overwhelming thing.

Last but not least, I want to thank all my family members and dad in heaven for letting me adventure what I wanted to.

Bibliography

[1] Frank Arute, Kunal Arya, Ryan Babbush, et al. "Quantum supremacy using a programmable superconducting processor". In: *Nature* 574 (2019), pp. 505–510. DOI: 10.1038/s41586-019-1666-5. URL: https://doi.org/10.1038/s41586-019-1666-5.

[2] *BBPSSW Distillation Circuit.* [Online image]. PaddlePaddle Quantum. 2021. URL: https://github.com/PaddlePaddle/Quantum/blob/master/tutorials/locc/figures/distillation-fig-BBPSSW.png.

[3] Charles H. Bennett et al. "Purification of Noisy Entanglement and Faithful Teleportation via Noisy Channels". In: *Physical Review Letters* 76.5 (Jan. 1996), pp. 722–725. ISSN: 1079-7114. DOI: 10.1103/physrevlett.76.722. URL: http://dx.doi.org/10.1103/PhysRevLett.76.722.

[4] Charles H. Bennett et al. "Teleporting an unknown quantum state via dual classical and Einstein-Podolsky-Rosen channels". In: *Phys. Rev. Lett.* 70 (13 Mar. 1993), pp. 1895–1899. DOI: 10.1103/PhysRevLett.70.1895. URL: https://link.aps.org/doi/10.1103/PhysRevLett.70.1895.

[5] Chris Bernhardt. *Quantum Computing for Everyone.* MIT Press, 2019. ISBN: 9780262539531. URL: https://mitpress.mit.edu/9780262539531/quantum-computing-for-everyone/.

[6] Boris B. Blinov et al. "Quantum Computing with Trapped Ion Hyperfine Qubits". In: *Quantum Information Processing* 3 (2004), pp. 45–59. URL: https://api.semanticscholar.org/CorpusID:22586758.

[7] L. Childress and R. Hanson. "Diamond NV centers for quantum computing and quantum networks". In: *MRS Bulletin* 38 (2013), pp. 134–138. DOI: 10.1557/mrs.2013.20. URL: https://doi.org/10.1557/mrs.2013.20.

[8] J. M. Chow et al. "Randomized Benchmarking and Process Tomography for Gate Errors in a Solid-State Qubit". In: *Physical Review Letters* 102.9 (Mar. 2009). ISSN: 1079-7114. DOI: 10.1103/physrevlett.102.090502. URL: http://dx.doi.org/10.1103/PhysRevLett.102.090502.

[9] Andrew Cross. "The IBM Q experience and QISKit open-source quantum computing software". In: *APS March Meeting Abstracts.* Vol. 2018. APS Meeting Abstracts. Jan. 2018, L58.003, p. L58.003.

[10] Giacomo Mauro D'Ariano and Lorenzo Maccone. "Quantum Tomography for Imaging". In: *Electronic Notes in Discrete Mathematics* 20 (2005). Proceedings of the Workshop on Discrete Tomography and its Applications, pp. 133–150. ISSN: 1571-0653. DOI: https://doi.org/10.1016/j.endm.2005.05.059. URL: https://www.sciencedirect.com/science/article/pii/S1571065305050638.

[11] P. A. M. Dirac. "A new notation for quantum mechanics". In: *Mathematical Proceedings of the Cambridge Philosophical Society* 35.3 (1939), pp. 416–418. DOI: 10.1017/S0305004100021162.

[12] David P. DiVincenzo. "The Physical Implementation of Quantum Computation". In: *Fortschritte der Physik* 48.9–11 (Sept. 2000), pp. 771–783. ISSN: 1521-3978. DOI: 10.1002/1521-3978(200009)48:9/11<771::aid-prop771>3.0.co;2-e. URL: http://dx.doi.org/10.1002/1521-3978(200009)48:9/11%3C771::AID-PROP771%3E3.0.CO;2-E.

[13] Artur K. Ekert. "Quantum Cryptography and Bell's Theorem". In: *Quantum Measurements in Optics.* Ed. by Paolo Tombesi and Daniel F. Walls. Boston, MA: Springer US, 1992, pp. 413–418. ISBN: 978-1-4615-3386-3. DOI: 10.1007/978-1-4615-3386-3_34. URL: https://doi.org/10.1007/978-1-4615-3386-3_34.

[14] Edward Farhi, Jeffrey Goldstone, and Sam Gutmann. *A Quantum Approximate Optimization Algorithm.* 2014. arXiv: 1411.4028 [quant-ph].

[15] Richard P. Feynman. “Simulating physics with computers”. In: *International Journal of Theoretical Physics* 21 (1982), pp. 467–488. DOI: 10.1007/BF02650179. URL: https://doi.org/10.1007/BF02650179.

[16] Nicolai Friis et al. “Observation of Entangled States of a Fully Controlled 20-Qubit System”. In: *Physical Review X* 8.2 (Apr. 2018). ISSN: 2160-3308. DOI: 10.1103/physrevx.8.021012. URL: http://dx.doi.org/10.1103/PhysRevX.8.021012.

[17] Keisuke Fujii and Katsuji Yamamoto. “Entanglement purification with double selection”. In: *Physical Review A* 80.4 (Oct. 2009). ISSN: 1094-1622. DOI: 10.1103/physreva.80.042308. URL: http://dx.doi.org/10.1103/PhysRevA.80.042308.

[18] Craig Gidney and Martin Ekerå. “How to factor 2048 bit RSA integers in 8 hours using 20 million noisy qubits”. In: *Quantum* 5 (Apr. 2021), p. 433. ISSN: 2521-327X. DOI: 10.22331/q-2021-04-15-433. URL: http://dx.doi.org/10.22331/q-2021-04-15-433.

[19] Vittorio Giovannetti, Seth Lloyd, and Lorenzo Maccone. “Advances in quantum metrology”. In: *Nature Photonics* 5.4 (Mar. 2011), pp. 222–229. ISSN: 1749-4893. DOI: 10.1038/nphoton.2011.35. URL: http://dx.doi.org/10.1038/nphoton.2011.35.

[20] Lov K. Grover. *A fast quantum mechanical algorithm for database search.* 1996. arXiv: quant-ph/9605043 [quant-ph].

[21] Michal Hajdušek and Rodney Van Meter. *Quantum Communications.* 2023. arXiv: 2311.02367 [quant-ph].

[22] M. Hein et al. *Entanglement in Graph States and its Applications.* 2006. arXiv: quant-ph/0602096 [quant-ph].

[23] A. A. Houck et al. “Life after charge noise: recent results with transmon qubits”. In: *Quantum Information Processing* 8.2–3 (Feb. 2009), pp. 105–115. ISSN: 1573-1332. DOI: 10.1007/s11128-009-0100-6. URL: http://dx.doi.org/10.1007/s11128-009-0100-6.

[24] IBM Cloud. *IBM Cloud Documentation.* Accessed: 2024/1/28. 2023. URL: https://cloud.ibm.com/docs/overview?topic=overview-notices.

[25] F. Jelezko and J. Wrachtrup. “Single defect centres in diamond: A review”. In: *physica status solidi (a)* 203.13 (2006), pp. 3207–3225. DOI: https://doi.org/10.1002/pssa.200671403. eprint: https://onlinelibrary.wiley.com/doi/pdf/10.1002/pssa.200671403. URL: https://onlinelibrary.wiley.com/doi/abs/10.1002/pssa.200671403.

[26] Abhinav Kandala et al. “Hardware-efficient variational quantum eigensolver for small molecules and quantum magnets”. In: *Nature* 549.7671 (Sept. 2017), pp. 242–246. ISSN: 1476-4687. DOI: 10.1038/nature23879. URL: http://dx.doi.org/10.1038/nature23879.

[27] E. Knill, R. Laflamme, and G. Milburn. *Efficient Linear Optics Quantum Computation.* 2000. arXiv: quant-ph/0006088 [quant-ph].

[28] Jens Koch et al. “Charge-insensitive qubit design derived from the Cooper pair box”. In: *Physical Review A* 76.4 (Oct. 2007). ISSN: 1094-1622. DOI: 10.1103/physreva.76.042319. URL: http://dx.doi.org/10.1103/PhysRevA.76.042319.

[29] P. Krantz et al. “A quantum engineer’s guide to superconducting qubits”. In: *Applied Physics Reviews* 6.2 (June 2019). ISSN: 1931-9401. DOI: 10.1063/1.5089550. URL: http://dx.doi.org/10.1063/1.5089550.

[30] N. Leung et al. *Deterministic Bidirectional Communication and Remote Entanglement Generation Between Superconducting Quantum Processors.* 2018. arXiv: 1804.02028 [quant-ph].

[31] Jin Li, Rajesh Pereira, and Sarah Plosker. “Some geometric interpretations of quantum fidelity”. In: *Linear Algebra and its Applications* 487 (Dec. 2015), pp. 158–171. ISSN: 0024-3795. DOI: 10.1016/j.laa.2015.08.037. URL: http://dx.doi.org/10.1016/j.laa.2015.08.037.

[32] Sheng-Kai Liao et al. “Satellite-to-ground quantum key distribution”. In: *Nature* 549.7670 (Aug. 2017), pp. 43–47. ISSN: 1476-4687. DOI: 10.1038/nature23655. URL: http://dx.doi.org/10.1038/nature23655.

[33] Ananda G. Maity et al. “Noise estimation in an entanglement distillation protocol”. In: *SIGMETRICS Perform. Eval. Rev.* 51.2 (Oct. 2023), pp. 66–68. ISSN: 0163-5999. DOI: 10.1145/3626570.3626594. URL: https://doi.org/10.1145/3626570.3626594.

[34] Jarrod R McClean et al. "The theory of variational hybrid quantum-classical algorithms". In: *New Journal of Physics* 18.2 (Feb. 2016), p. 023023. ISSN: 1367-2630. DOI: 10.1088/1367-2630/18/2/023023. URL: http://dx.doi.org/10.1088/1367-2630/18/2/023023.

[35] Rodney Van Meter et al. "Arithmetic on a distributed-memory quantum multicomputer". In: *ACM Journal on Emerging Technologies in Computing Systems* 3.4 (Jan. 2008), pp. 1–23. ISSN: 1550-4840. DOI: 10.1145/1324177.1324179. URL: http://dx.doi.org/10.1145/1324177.1324179.

[36] Y. Nakamura, Yu. A. Pashkin, and J. S. Tsai. "Coherent control of macroscopic quantum states in a single-Cooper-pair box". In: *Nature* 398.6730 (Apr. 1999), pp. 786–788. ISSN: 1476-4687. DOI: 10.1038/19718. URL: http://dx.doi.org/10.1038/19718.

[37] P. J. J. O'Malley et al. "Scalable Quantum Simulation of Molecular Energies". In: *Phys. Rev. X* 6 (3 July 2016), p. 031007. DOI: 10.1103/PhysRevX.6.031007. URL: https://link.aps.org/doi/10.1103/PhysRevX.6.031007.

[38] Jian-Wei Pan, S. Gasparoni, Rupert Ursin, et al. "Experimental entanglement purification of arbitrary unknown states". In: *Nature* 423 (2003), pp. 417–422. DOI: 10.1038/nature01623. URL: https://doi.org/10.1038/nature01623.

[39] Alberto Peruzzo, Jarrod McClean, Peter Shadbolt, et al. "A variational eigenvalue solver on a photonic quantum processor". In: *Nature Communications* 5 (2014), p. 4213. DOI: 10.1038/ncomms5213. URL: https://doi.org/10.1038/ncomms5213.

[40] John Preskill. "Quantum Computing in the NISQ era and beyond". In: *Quantum* 2 (Aug. 2018), p. 79. ISSN: 2521-327X. DOI: 10.22331/q-2018-08-06-79. URL: http://dx.doi.org/10.22331/q-2018-08-06-79.

[41] Qiskit Development Team. *Qiskit Experiments GitHub Repository.* https://github.com/Qiskit-Extensions/qiskit-experiments. Accessed: 2024/1/28. 2024.

[42] Qiskit Development Team. *Qiskit GitHub Repository.* https://github.com/Qiskit. Accessed: 2024/1/28. 2024.

[43] M. Sasaki et al. "Field test of quantum key distribution in the Tokyo QKD Network". In: *Optics Express* 19.11 (May 2011), p. 10387. ISSN: 1094-4087. DOI: 10.1364/oe.19.010387. URL: http://dx.doi.org/10.1364/OE.19.010387.

[44] Peter W. Shor. "Polynomial-Time Algorithms for Prime Factorization and Discrete Logarithms on a Quantum Computer". In: *SIAM Journal on Computing* 26.5 (1997), pp. 1484–1509. DOI: 10.1137/S0097539795293172. URL: https://doi.org/10.1137/S0097539795293172.

[45] R.S. Sutor. *Dancing with Qubits: How Quantum Computing Works and how it Can Change the World.* Expert Insight. Packt Publishing, 2019. ISBN: 9781838827366. URL: https://books.google.co.jp/books?id=uwAeywEACAAJ.

[46] Guifré Vidal. "Efficient classical simulation of slightly entangled quantum computations". In: *Physical Review Letters* 91.14 (Oct. 2003), p. 147902. DOI: 10.1103/physrevlett.91.147902.

[47] Haoxiong Yan et al. "Entanglement Purification and Protection in a Superconducting Quantum Network". In: *Physical Review Letters* 128.8 (Feb. 2022). ISSN: 1079-7114. DOI: 10.1103/physrevlett.128.080504. URL: http://dx.doi.org/10.1103/PhysRevLett.128.080504.

[48] Xiao-Dong Yu, Jiangwei Shang, and Otfried Gühne. "Statistical Methods for Quantum State Verification and Fidelity Estimation". In: *Advanced Quantum Technologies* 5.5 (Mar. 2022). ISSN: 2511-9044. DOI: 10.1002/qute.202100126. URL: http://dx.doi.org/10.1002/qute.202100126.

[49] Youpeng Zhong et al. "Deterministic multi-qubit entanglement in a quantum network". In: *Nature* 590.7847 (Feb. 2021), pp. 571–575. ISSN: 1476-4687. DOI: 10.1038/s41586-021-03288-7. URL: http://dx.doi.org/10.1038/s41586-021-03288-7.